AD-A203 050

THE CONTROL RECONFIGURABLE COMBAT AIRCRAFT DESIGNED USING QUANTITATIVE FEEDBACK THEORY

THESIS

Kurt Nyle Neumann
Captain, USAF

AFIT/GE/ENG/88D-33

DEPARTMENT OF THE AIR FORCE

AIR UNIVERSITY

AIR FORCE INSTITUTE OF TECHNOLOGY

Wright-Patterson Air Force Base, Ohio

89   1 17   164

AFIT/GE/ENG/88D-33

A DIGITAL RATE CONTROLLER FOR
THE CONTROL RECONFIGURABLE COMBAT
AIRCRAFT DESIGNED USING QUANTITATIVE
FEEDBACK THEORY

THESIS

Kurt Nyle Neumann
Captain, USAF

AFIT/GE/ENG/88D-33

AFIT/GE/ENG/88D-33

A DIGITAL RATE CONTROLLER FOR THE CONTROL RECONFIGURABLE COMBAT AIRCRAFT DESIGNED USING QUANTITATIVE FEEDBACK THEORY

THESIS

Presented to the Faculty of the School of Engineering

of the Air Force Institute of Technology

Air University

In Partial Fulfillment of the

Requirements for the Degree of

Master of Science in Electrical Engineering

Kurt Nyle Neumann, B.A., B.S.E.E.

Captain, USAF

December, 1988

Acknowledgments

To my wife, Susan. If I ever mention getting another degree, please remind me of all the good times we had at AFIT.

Kurt Nyle Neumann

ii

Table of Contents

List of Figures

List of Tables

AFIT GE ENG 88D

Abstract

The objective of this thesis is to develop a digital controller using Quantitative Feedback Theory for a fighter aircraft with unstable, nonminimum phase dynamics that meets performance specifications despite surface failures. Aircraft design trends for highly manueverable fighter aircraft are relaxing stability requirements in order to increase performance in the transonic and supersonic regions. However, as a result, the aircraft is statically unstable in the subsonic region which makes the flight control system critical to flight safety. The conventional approach to the flight safety problem is to provide multiple redundancy throughout the flight control system. However, QFT provides an alternative to excessive hardware.

The three controlled states are the pitch, roll, and yaw rates. A weighting matrix is derived which linearly combines the nine control surfaces into three control inputs. The plant is converted to the w plane using the Hoffman algorithm. Three constant gain controllers and three prefilters are designed for a single flight condition of 0.9 Mach and 30000 ft altitude. The controllers and prefilters are transformed to the z plane for simulation purposes. The design is simulated with a healthy plant and 24 combinations of surface failures. The failure cases consisted of single and double surface impairments. The nonlinear effects of rate and deflection limiters on the actuator models are added to the simulations. The first set of simulations consist of single channel inputs to determine the level of inertial decoupling. A coordinated turn with 55 degrees of bank is simulated next. The first order actuators are replaced with fourth order actuators and a digital filter is cascaded with the digital controllers. The loop transmission is nearly restored and a 2 degree/second pitch rate command and 90 degree/second roll command are simulated. An attempt to extend the design to a second flight condition of 0.9 Mach and 200 ft is unsuccessful.

The design is shown to meet design objectives in spite of surface failures for all failure conditions in the longitudinal mode. Two failure conditions are not satisfactorily controlled during the roll rate commands. The replacement of the first order actuators with the fourth order actuators is shown to be most successful in the longitudinal mode. Excessive oscillatory behavior is found in the lateral modes. Quantitative Feedback Theory is shown to be applicable for sampled-data, multi-input, multi-output, unstable, and nonminimum phase aircraft.

A DIGITAL RATE CONTROLLER FOR THE CONTROL RECONFIGURABLE COMBAT AIRCRAFT DESIGNED USING QUANTITATIVE FEEDBACK THEORY

I. Flight Control System Design

Introduction

The aircraft flight control system (FCS) has evolved into a highly redundant, flight-critical, and maintenance intensive system at the expense of aircraft performance [5]. On current high performance aircraft, the conventional FCS design approach has resulted in large, high authority control aerosurfaces to generate the rotational moments needed for both performance and flight safety [5]. Failure of any of these surfaces can result in a loss of control in the affected dimension and probable loss of the aircraft. Air Force operational policy is a result of the criticality of the FCS; no aircraft can start a mission without a 100% operational FCS and the FCS must be able to withstand two failures during a mission without any loss of capability [5]. The costs imposed by such requirements on the FCS are weight, complexity, and reliability which directly affects payload, range, and performance [5]. If the value of any one aerosurface in terms of flight safety could be reduced without a loss in performance, then the damage of that surface might be sustained without the potential loss of the mission or the aircraft. One method of reducing the value of a control surface is to design an FCS which is tolerant of control surface damage. In other words, the FCS design should continue to meet the performance specifications despite an uncertainty in the available control force from a control surface. Such a reduction in the criticality of a control surface would

allow the simplification of the design of many of the components of the FCS with a parallel increase in mission effectiveness.

Quantitative Feedback Theory (QFT) is a design approach which specifically confronts the problem of uncertainty in feedback systems in a manner which encourages the explicit trade-off of design parameters. The philosophy behind QFT is firmly rooted in the classical frequency approach to feedback design. As Professor Horowitz points out in his book, *Synthesis of Feedback Systems*, the use of feedback is motivated by uncertainty of the plant dynamics, plant parameters, and plant inputs in the form of disturbances. This uncertainty causes the desired plant output and actual plant output to be different. Feedback is employed to compare the intended output with the actual output and adjust the input to the plant accordingly [10]. The difficulty lies in determining how much feedback to employ; too little feedback and the uncertainty is not adequately controlled and too much feedback and the loop bandwidth increases to an unacceptable level. However, QFT optimizes the amount of feedback for a given amount of parameter uncertainty [11,12,13,14,16]. The optimization process is accomplished by examining the costs and benefits of feedback across the frequency spectrum of interest.

One of the first decisions which must be made in the design of a control system is to determine the amount of uncertainty which will be controlled [17,19]. The level of feedback required increases with increasing uncertainty. Eventually, the amount of controllable uncertainty is limited by the maximum permissible loop bandwidth. This example is typical of a control system design; the continual balancing of competing requirements. The advantage of the QFT approach is that many of the trade-offs are explicit. The design choices are made with the impact on design parameters such as bandwidth, noise susceptibility, or phase margin clearly defined. This transparency makes QFT ideally suited for designing an aircraft FCS.

Problem Description

The Control Reconfigurable Combat Aircraft (CRCA) project at the Air Force Wright Aeronautical Laboratory (AFWAL) Flight Dynamics Laboratory (FDL) is an ongoing effort to integrate a robust flight control system with a failure detection system. The aircraft model is a hypothetical advanced tactical aircraft modeled in a six degree-of-freedom nonlinear simulation. The existing flight control system is a proportional plus integral (PI) controller in the feed-forward loop for both the longitudinal and lateral axes [26]. While the current FCS meets or exceeds most of the requirements for a category II (fighter) aircraft, several areas for improvement exist. Specifically, unnecessary pitch rate overshoot is evident and yaw and roll rates are coupled under certain failure conditions. The purpose of this thesis is to replace the existing flight control system with one designed using QFT without a reliance on a failure detection system. The primary goal for this thesis is to minimize pitch rate overshoot and decouple yaw and roll rates in spite of control surface failure. A secondary goal is to demonstrate the applicability of QFT to an unstable, nonminimum phase, sampled-data flight control system.

Background

Advanced fighter design concepts are relaxing the static stability requirements in both the longitudinal and lateral axes to improve transonic and supersonic performance [4,26]. The F-16, the AFTI F-16, and the X-29 are examples of aircraft which are unstable in the longitudinal axis. In addition, dynamic analysis of modern fighter aircraft reveals that unacceptable levels of inertial cross-coupling can occur during certain manuevers such as high-speed rolls [7]. The combination can place such large demands on the control system that the FCS becomes the limiting factor on aircraft performance. For instance, enhancing transonic performance by moving the center of gravity backwards is limited by the necessity of maintaining sufficient nose-down pitching moment in high angle of attack manuev-

1-3

ers to prevent departure. In addition to maintaining control during a commanded input, sufficient control power must also exist at all points in the flight envelope to counter the effects of inertial cross-coupling, airframe instabilities, and turbulence [4]. The control surfaces can be increased in size to generate larger rotational moments, but with the attendant cost of increasing the criticality of the aerosurfaces. If the surface size is increased to provide the control power necessary to maintain stability, then the loss of that surface will precipitate the loss of control of the aircraft.

The objective of a FCS design for a statically unstable aircraft is to provide adequate control power to meet the performance requirements while minimizing overdesign of the FCS without compromising flight safety. The increased performance capabilities must be balanced against the adverse effects caused by stabilizing the divergent airframe roots [4]. Obviously, a 10 g aircraft which cannot adequately reject disturbance inputs is not a high performance aircraft. In addition, the design must also take into account the performance limitations of the hardware and uncertainty in the plant parameters. A design which requires unrealistic control surface deflections to meet performance requirements or does not control the plant throughout the flight envelope is obviously unacceptable. Performance vs disturbance rejection and performance vs hardware limitations are two examples of the kinds of trade-offs faced in the design of a FCS. The difficulty lies in relating these trade-offs to design parameters such as bandwidth and how a particular design step impacts the outcome of a trade-off.

A flight control system must manage numerous dynamic uncertainties. The healthy aircraft is subjected to plant parameter variation due to dynamic loading and noise inputs due to gusts. In addition, partially understood structural modes, sensor noises, and unknown effects due to aging further complicate the design process. Finally, an aircraft with damaged control surfaces is subjected to even further plant parameter variations. One approach to the design of a FCS is to quantify the

amount of uncertainty before the design process begins. For instance. the dynamic effects of a missing surface can be predicted with wind tunnel data derived from a model with the surface removed. Once a set of dynamic equations describing a range of plant variations is derived, a controller which is tolerant to the set of modeled impairments can be designed. At the same time, equal importance should be placed on reducing the amount of overdesign in the controller. Overdesign is defined as providing more feedback than necessary to reduce the plant sensitivity to a parameter variation [10]. If the flight control system is robust to parameter variations and has a minimal amount of overdesign, the overall complexity of the flight control system could be reduced. The objectives of the CRCA program are to increase reliability, ease maintainability, and increase weapon effectiveness. These objectives are attainable at least in part by using a flight control system designed using QFT.

The loop bandwidth of flight control system is one measure of how well the desired objectives are balanced against the imposed costs of feedback. The bandwidth defines the frequency range where the open-loop gain must be greater than one in order to obtain good system performance while maintaining tractable disturbance rejection characteristics [4]. As the bandwidth is increased, the amount of disturbance rejection increases. However,the response of the plant to high frequency components such as sensor noise and structural modes is also increasing. If the bandwidth becomes too large, the control system can introduce high frequency flutter to the aerosurfaces which can lead to saturation of the actuators. The obvious trade-off is to maximize bandwidth until the frequency range of the sensor noise or structural modes are encountered. The obstacle for many design approaches lies in finding precise relationships between the desired design measures of merit and specific design steps. QFT on the other hand is particularly well suited to explicitly describing the relationship between frequency design specifications such as gain margin or phase margin and controller design. The effect

of adding a pole or zero to the controller on bandwidth, phase or gain margin, or crossover frequency is graphically portrayed when the loop transmission is plotted on the Nichols chart. Trade-offs can be made with the benefits and costs explicitly shown.

One example of how QFT is ideally suited to FCS design is demonstrated by displaying the limits on the amount of uncertainty that the use of feedback can control. Templates are used in QFT to graphically portray the phase angle and magnitude characteristics of a transfer function with a range of uncertainty at a particular frequency. The larger the uncertainty, the larger the template tends to become. The templates are used to determine the stability and performance bounds which guide the shaping of the loop transmission function. As the size of the templates increase, the resultant bounds force the frequency of the crossover point to increase. The open loop crossover point is a rough approximation of where the dynamics of the closed loop system starts to attenuate rather than amplify information from the higher frequencies. If the bandwidth extends into the regions where noise or structural modes dominate, then the costs of feedback have overwhelmed the desired benefits. Therefore, the templates allow the designer to set realistic performance goals graphically revealing the limitations of feedback.

A second example of how QFT is applicable to the design of flight control systems is in the area of stability margins. The military design specification mil std 9490D requires a high frequency gain margin of 6 dB. The stability margins are built into the design to cope with unmodeled aspects of the plant such as higher order dynamics or sensor noise [4]. If the design technique employed does not allow visibility into characteristics such as the loop transmission frequency response, the compensator may meet performance specifications but might be overdesigned. In such a case, the frequency response of the loop transmission function will needlessly extend into the higher frequencies. The result can be excessive high frequency noise amplification and potential plant saturation. QFT avoids this situation during the

loop shaping process. Loop shaping is performed by plotting the loop transmission function on a Nichols chart. The performance specifications are embedded in design equations which are used to plot boundaries on the Nichols chart. The compensator is designed to meet the performance boundaries within the constraints of the stability margins. A choice for the compensator is quickly shown to be adequate based on the loop transmission plot relative to the performance bounds. As the compensator is developed, critical design parameters such as gain margin or susceptibility to noise amplification are continually displayed on the chart. Overdesign is avoided since the amount of feedback can be fine-tuned with respect to the design parameters. The "guess and simulate" approach is unnecessary and design time is greatly reduced.

Approach

The development of this thesis is broken into several parts. First, the basic plant models for the nominal case and the failure set are derived from aerodynamic derivatives. Second, a weighting matrix is derived which linearly combines the nine columns of the input matrix into three columns. Third, the continuous plant and actuators are transformed to the discrete $w\prime$ plane. Fourth, the three compensators are designed in the $w\prime$ plane using the Quantitative Feedback Theory approach. Finally, the closed loop system is simulated in the z plane using the dynamic system modeling capabilities of MatrixX.

Assumptions

The following assumptions form the basis from which the work performed in this thesis is begun.

1. The aerodynamic data supplied by AFWAL/FDL adequately represents the aircraft.

2. The software provided by AFWAL/FDL used to obtain the linear aircraft state space model operates correctly.

3. The fixed sampling rate of 80 Hz is sufficient.

4. The mass of the aircraft remains constant throughout the simulation time period.

5. The aircraft engine thrust remains constant through the simulation time period.

6. The aircraft can be treated as a rigid body for the purposes of deriving the linear equations of motion.

7. The earth surface is the inertial reference frame.

8. The atmosphere is fixed to the surface of the earth.

9. No failure detection schemes will be employed to augment the constant gain controller to maintain stability.

10. The actuators have no uncertainty across the frequency spectrum.

11. Effects of finite wordlength will not be investigated.

Presentation

This thesis is divided into six chapters. The development of the basic aircraft model in the s plane and the weighting matrix derivation are presented in chapter 2. The third chapter presents the effective plant development in the $w\prime$ plane and the digital QFT design procedures. Chapter 4 presents the design of the digital compensators and prefilters. Simulation results are presented in chapter 5. Finally, conclusions and recommendations are presented in the sixth chapter.

II. Model Development

Overview

The objective of this chapter is to outline the procedures used to develop the basic plant transfer function matrix, the weighting matrix, and the effective plant transfer function matrix in the continuous s plane. The basic plant is defined as the $8x9$ transfer function matrix. The effective plant is defined as basic plant postmultiplied by the weighting matrix. Three states are used in feedback so the final transfer function matrix is a square $3x3$ matrix. A linear state space model of the aircraft is derived. The equivalent basic plant transfer function matrix is obtained in the continuous s plane. A weighting matrix is developed which linearly combines the nine columns of the input matrix into three columns. The effective plant is derived in the continuous plane by postmultiplication of the plant matrix with the weighting matrix. The actuators are cascaded with the effective plant model. The effective plant is transformed to the w' plane and the determinant of the $3x3$ transfer function matrix is taken. The effective plant is shown to be minimum phase for 25 of the potential 28 failure cases for one aerodynamic flight condition and for 16 of 17 potential failure cases for a second aerodynamic flight condition.

Aircraft Description

The CRCA is a modified version of a NASA/Grumman advanced tactical fighter (ATF) class aircraft model. The CRCA is a "paper airplane"; a math model simulated on the Air Force Simulation/Rapid-Prototyping Facility located at the Air Force Wright Aeronautical Laboratories (AFWAL) Flight Dynamics Laboratory (FDL). The aircraft is representative of a 1995 fighter type aircraft. At low airspeeds, the aircraft is 12% unstable in the longitudinal mode. There are nine control surfaces: two canards with thirty degrees of dihedral, four trailing-edge

2-1

flaps. two elevators. and a rudder. The canards provide the main pitch moment and a smaller amount of yaw and roll moments. The two trailing-edge flaps on each wing are used to provide both rolling and yawing moments. The two elevators provide both pitch and roll moments. The rudder supplies yaw moment [26].
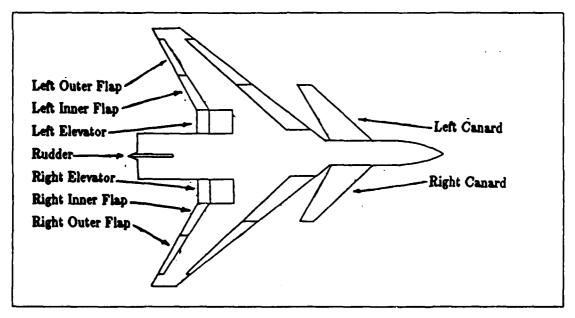
Figure 2.1. Control Reconfigurable Combat Aircraft

The design for this thesis is developed using data provided for the Air Combat Manuever (ACM) Entry condition. The condition represents the aerodynamic effects of a fighter maneuvering at 0.9 Mach at 30000 ft. Combat maneuvering requires the aircraft to roll rapidly without inducing a loss of control due to inertial cross-coupling, to quickly induce maximum g-loading, and to maintain coordination to reduce drag. The initial aircraft orientation is the trim condition with the wings level. After completion of the design, the unmodified controller is also simulated in the Terrain-Following, Terrain-Avoidance (TFTA) condition. The two conditions are similar in terms of g loading but the Q factor (dynamic loading) for the TFTA manuever is much larger. The TFTA represents the effects of flying at 200 ft at 0.9 Mach at low angles of attack with rapid but limited changes in pitch angle and bank angle [26].

Basic Plant

The trim or nominal case and subsequent failure cases are developed from nondimensional aerodynamic derivatives. The derivatives are the result of a nonlinear simulation of the aircraft drawing on a database made up of a blend of wind tunnel data and the estimated aerodynamic effects of partial aerosurface losses. The aircraft surfaces were trimmed to balance the resulting moments and the thrust was adjusted to compensate for any change in drag to maintain the initial velocity. The nonlinear equations of motion were then perturbed about an equilibrium point to generate the nondimensional aerodynamic derivatives. The derivatives were supplied to the author by AFWAL/FDCL.

The linear equations of motion are developed using two programs provided by AFWAL/FDCL [3] The first program uses the nondimensional coefficients as input data to derive the dimensional coefficients. The second program uses the dimensional coefficients to develop the linear state equations. The linear equations of motion are developed in the standard state space format of

$$\dot{\overline{x}} = \overline{A}\,\overline{x} + \overline{B}\,\overline{u}$$

$$\overline{y} = \overline{C}\,\overline{x} + \overline{D}\,\overline{u} \tag{2.1}$$

where $\overline{x}$ is an 9x1 state variable vector.

$\overline{u}$ is a 9x1 state input vector.

$\overline{A}$ is an 9x9 state dynamics matrix.

$\overline{B}$ is an 9x9 state input matrix.

$\overline{C}$ is a 3x9 state output matrix.

$\overline{D}$ is a 3x9 state feed forward matrix.

The state variable vector for the CRCA is given by

$$\bar{x} = \begin{bmatrix} u \\ w \\ q \\ \theta \\ \psi \\ \phi \\ \beta \\ p \\ r \end{bmatrix} \tag{2.2}$$

The state control input vector for the CRCA is given by

$$\bar{u} = \begin{bmatrix} left\ canard \\ right\ canard \\ left\ outer\ flap \\ left\ inner\ flap \\ right\ outer\ flap \\ right\ inner\ flap \\ left\ elevator \\ right\ elevator \\ rudder \end{bmatrix} \tag{2.3}$$

The linear state space model consists of a nine state A matrix and a nine input B matrix. The A matrix is block diagonal indicating the longitudinal and lateral modes are decoupled. The B matrix is not diagonal; most control inputs affect both the longitudinal and lateral states; the only single axis surface is the rudder. The A matrix is rank deficient so the equation

$$\dot{\psi} = r \tag{2.4}$$

is removed by deleting the fifth row and fifth column of the A matrix and the fifth row of the B matrix. The A matrix is now full rank and therefore invertible. The

2-4

A matrix is now 8x8, the B matrix is 8x9. and the state vector is 8x1. The A matrix for the nominal condition of the ACM manuever is given by:

$$
\begin{bmatrix}
-0.008 & 0.054 & -31.547 & -32.154 & 0 & 0 & 0 & 0 \\
-0.032 & -1.058 & 894.4 & -1.134 & 0 & 0 & 0 & 0 \\
0 & 0.007 & -0.663 & 0 & 0 & 0 & 0 & 0 \\
0 & 0 & 1.0 & 0 & 0 & 0 & 0 & 0 \\
0 & 0 & 0 & 0 & 0 & 0 & 1.0 & 0.035 \\
0 & 0 & 0 & 0 & 0.036 & -0.093 & 0.035 & -0.999 \\
0 & 0 & 0 & 0 & 0 & -27.855 & -2.041 & 0.492 \\
0 & 0 & 0 & 0 & 0 & 2.462 & -0.024 & -0.438
\end{bmatrix}
\tag{2.5}
$$

The B matrix for the nominal condition is given by:

$$
\begin{bmatrix}
0.041 & 0.041 & 0.132 & 0.087 & 0.132 & 0.087 & 0.102 & 0.102 & 0 \\
-0.317 & -0.317 & -.960 & -0.620 & -0.960 & -0.620 & -0.733 & -0.733 & 0 \\
0.102 & 0.102 & -0.028 & -0.022 & -0.028 & -0.022 & -0.020 & -0.020 & 0 \\
0 & 0 & 0 & 0 & 0 & 0 & 0 & 0 & 0 \\
0 & 0 & 0 & 0 & 0 & 0 & 0 & 0 & 0 \\
0 & 0 & 0 & 0 & 0 & 0 & 0 & 0 & 0.001 \\
0.076 & -0.076 & 0.222 & 0.201 & -0.222 & -.201 & 0.111 & -0.111 & 0.115 \\
0.049 & -0.049 & 0.003 & 0.002 & -0.003 & -.002 & 0.002 & -0.002 & 0.054
\end{bmatrix}
\tag{2.6}
$$

The three state variables which are controlled by feedback are roll rate, pitch rate, and yaw rate. The required C matrix is then given by:

$$
\begin{bmatrix}
0 & 0 & 1.0 & 0 & 0 & 0 & 0 & 0 \\
0 & 0 & 0 & 0 & 0 & 0 & 1.0 & 0 \\
0 & 0 & 0 & 0 & 0 & 0 & 0 & 1.0
\end{bmatrix}
\tag{2.7}
$$

Since there are no feed-forward terms the D matrix is a 3x9 zero matrix.

Using the expression,

$$
\frac{Y(s)}{U(s)} = C(s)(sI - A)^{-1}B(s) + D(s)
\tag{2.8}
$$

Aerosurface	Deflection Limit		Rate Limit
Canards	-60 degrees	-30 degrees	100 degrees/second
Trailing Edge Flaps	$+30$ degrees	-30 degrees	100 degrees/second
Rudder	$+20$ degrees	-20 degrees	100 degrees/second

Table 2.1. Deflection and Rate Limits

the corresponding transfer functions for the basic nine-input, three-output plant are derived [6]. The basic plant transfer functions are in appendix C. The transfer functions for the commanded pitch rate have an unstable root at $s = 1.694$. The commanded roll rate transfer functions are stable with a small nonminimum phase zero. The commanded yaw rate transfer functions are also stable but with two right half plane complex zeros.

The actuators for the CRCA are modeled using two fourth order approximations. The actuators for the canards and flaps are modeled by:

$$\frac{Y(s)}{U(s)} = \frac{1.1816 \cdot 10^7}{(s + 20.20)(s + 52.55 \pm j48.34)(s + 114.7)} \tag{2.9}$$

The actuator for the rudder is modeled by:

$$\frac{Y(s)}{U(s)} = \frac{1.1551 \cdot 10^7}{(s + 20.6)(s - 54.1 \pm j46.1)(s + 111)} \tag{2.10}$$

The deflection and rate limits for the control surfaces are supplied by AFWAL/FDCL and are given in Table 2.1.

A linear simulation of the step response of both models is performed. The results in Figure 2.2 show that the two models have virtually identical time responses to step inputs. Therefore, the rudder actuator model is replaced by the canard or flaperon actuator model with no loss of fidelity. The actuator model is cascaded with each basic plant transfer function and is considered to have no uncertainty throughout the frequency range.
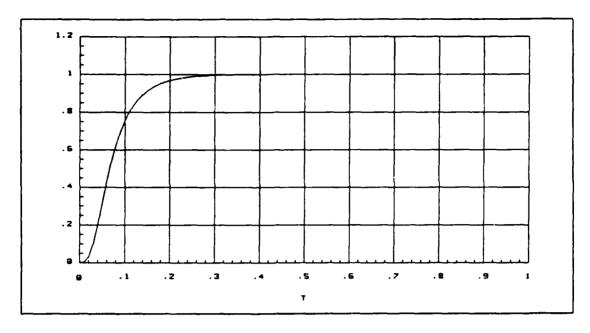
Figure 2.2. Time Response of Canard/Flaperon and Rudder Actuator Models

Failure Cases

The aerodynamic data for 27 simulated single and double surface failures for the ACM entry manuever and 17 simulated failures for the TFTA manuever was supplied by the AFWAL/FDCL. The data is used to derive the corresponding state space models using the same approach described for the nominal case. The complete set for each aerodynamic condition consisting of the trimmed, unimpaired case and the simulated surface failures is referred to in this thesis as the design set. The simulated failures are loss-of-effectiveness failures and fail-to-trail failures of single and double surfaces. The loss-of-effectiveness failures simulate battle damage which removes 25%, 50%, and 100% of the affected aerosurface. The fail-to-trail failures simulate a surface locked at 0.7 times the local angle of attack. The complete list is located in appendix B.

The transfer functions derived from the design set for ACM entry are used to develop the templates. The templates are used to develop the stability boundaries. Once a control system is designed which meets the stability boundaries, the closed

loop system is simulated with the complete design set. The objective is to examine the ability of the constant gain QFT controller to continue meeting performance goals in spite of parameter variation due to surface failures.

Development of the Weighting Matrix

A weighting matrix is developed which converts the basic plant transfer function matrix into a $3x3$ effective plant transfer function matrix. The requirement for a square transfer function matrix is due to the manner in which QFT approaches the multi-input. multi-output (MIMO) design problem. An integral step of the design procedure is to convert a nxn plant into n^2 multi-input, single-output (MISO) plants. The conversion process requires the inversion of the MIMO plant matrix. Therefore, the MIMO transfer function matrix must be square. The weighting matrix must accomplish two unrelated objectives. First, the weighting matrix combines the terms of the control input matrix so that the determinant of the effective plant matrix is minimum phase for each member of the design set. Second, the weighting matrix spreads the control authority required to achieve the desired output across multiple control surfaces. Both goals are accomplished by linearly combining the nine columns of the input control matrix into three columns and thereby creating a three input control matrix.

The first objective for the weighting matrix is necessary in order to meet the performance specifications. The beneficial effects of feedback such as disturbance rejection are greatly reduced if the MIMO plant is not minimum phase. An MIMO plant is defined to be minimum phase if the determinant of the plant numerator matrix has no roots in the right-half plane [10]. The explanation for the reduction in performance of a nonminimum phase plant lies in the phase response of a transfer function due the nonminimum phase zero. At arbitrarily low frequencies, a minimum phase simple zero makes a phase contribution of zero degrees, but a nonminimum phase zero makes a phase contribution of 180 degrees. As the frequency
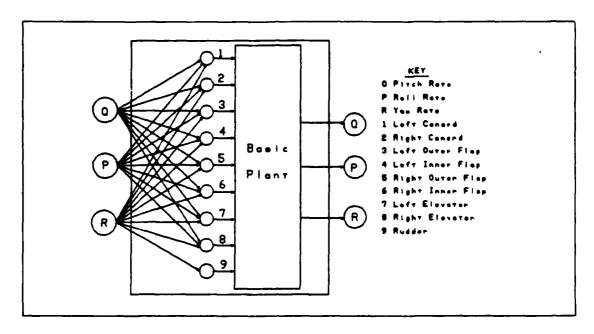
Figure 2.3. Effective Plant

increases. the minimum phase zero begins to increase in phase until a maximum of 90 degrees is reached. On the other hand, the nonminimum phase zero will decrease in phase until 90 degrees is also reached. Therefore, at low frequencies, the phase margins required for stability are eroded by a nonminimum phase zero and consequently the gain may need to be lowered to maintain stability. The lowered gain reduces the bandwidth over which the beneficial effects of feedback can operate and accordingly performance is reduced.

The second objective for the weighting matrix is to disperse the total required moment for a given input across multiple control surfaces. The pilot inputs to the closed loop CRCA for this thesis are pitch, roll, and yaw rate. However, the actual control inputs to the aircraft are the nine aerosurface movements. The weighting matrix translates the desired pilot inputs into control inputs for the CRCA by taking advantage of the multiaxis response of most of the CRCA surfaces. All surfaces except the rudder are used to implement a pitch or roll rate command and all the surfaces are used for the yaw command. Therefore, all the surfaces are employed to implement a pilot command. The individual terms of the weighting

matrix determine the level of effort required of each surface for each pilot command. The magnitude and signs of the weighting matrix terms must be such that the resulting aerosurface movements are coordinated and the deflections are within reasonable limits for given desired output. An additional feature of the weighting matrix is the criticality of any particular surface can be reduced by spreading control authority across multiple surfaces. If a surface is impaired, the required moments can still be generated by the remaining surfaces. The reconfigurability of the control inputs paths allows aircraft performance to degrade in incremental steps with multiple surface failures.

The conversion from the basic plant to an effective plant is accomplished by post-multiplying the basic plant transfer function matrix by the weighting matrix in the continuous s plane.

$$\frac{Y(s)}{U(s)} = \left\{ C(s)(sI - A)^{-1}B(s) + D(s) \right\} \cdot \Delta \tag{2.11}$$

Since the D matrix is a matrix of zeros, only the B matrix is post-multiplied by the weighting matrix.

Techniques for deriving the terms of the weighting matrix can be best described as opaque. Earlier QFT MIMO thesis efforts relied on previous experience and aerodynamic insight to determine the weightings for a surface. However, a recent thesis developed a method for determining the relative magnitudes of the weighting matrix elements. The method is called Specified Output because the weighting matrix is derived based on the desired steady state output [8]. The expression for the effective plant, $P_e(s)$, in the s plane is given by

$$P_e(s) = P_b(s) \cdot \Delta \tag{2.12}$$

In the steady state, if input equals the output, then the left hand side of the expression in equation (2.12) can be viewed as equivalent to a 3x3 identity matrix. At the same time, zeros in the off-diagonal positions indicates the lack of coupling between the commanded state and the other two uncommanded states.

If the product of the two terms on the right of the expression in equation (2.12) is an identity matrix, then delta must be equal to the inverse of $P_b(s)$. But since $P_b(s)$ is a 3x9 matrix and is not invertible, a pseudoinverse must be used [8]. The pseudoinverse is defined as

$$\{P_b(s)\}^{-1} = \left\{ P_b^t(s) \cdot P_b(s) \right\}^{-1} \cdot P_b^t(s) \tag{2.13}$$

Manipulating the Laplace form of the plant transfer functions to develop the weighting matrix is extremely cumbersome. Instead, the weighting matrix for this thesis is developed numerically by substituting jw for s in the plant transfer function matrices used in equation (2.13). The magnitude of the resulting complex value of equation (2.13) is found for five frequencies: $w = 1, 2, 4, 8$, and 16 rad/sec. The five magnitudes are summed and the average determined. The signs of the individual weighting matrix terms are determined by examination of the frequency response of the 27 transfer functions of the basic plant [17]. Multiplication of a term by -1 is used to force like aerosurfaces (left canard, right canard and so on) to have similar phase characteristics which indicates the surfaces are working together. The sign convention is overlaid on the magnitude terms. The result is normalized by some arbitrary factor to avoid heavily weighting the control surfaces in terms of surface deflection rates or angles. The weighting matrix derived for this thesis is

$$\begin{bmatrix} -3.2851 & 0.1685 & 3.5208 \\ -3.2851 & -0.1685 & -3.5208 \\ 0.9181 & 0.5902 & 1.0061 \\ 0.7191 & 0.5349 & 0.8647 \\ 0.9181 & -0.5902 & 1.0061 \\ 0.7191 & -0.5349 & -0.8647 \\ 0.6566 & 0.2947 & 0.5354 \\ 0.6566 & -0.2947 & -0.5354 \\ 0 & 0 & -3.1613 \end{bmatrix} \tag{2.14}$$

The derivation of the weighting matrix using the method described does not claim to be the optimal approach. If dynamics are used rather than only magnitudes for the individual elements, the phase and magnitude characteristics of like surfaces could be matched closely over a large frequency range. However, the objective of this thesis is to derive an adequate matrix and not the optimal matrix. The criteria for an adequate matrix are to produce a minimum phase determinant of the effective plant for each member of the design set in the discrete domain. The determinant of the effective plant is minimum phase if there are no right half plane zeros; this definition is slightly modified in the discrete w plane and is further discussed in the next chapter. Using the weighting matrix in equation (2.14), the determinant of the effective plant is shown in the next chapter to be minimum phase for the nominal case for both ACM entry and TFTA and for 24 of the possible 27 cases for the ACM manuever entry and for 16 of the 17 cases for the TFTA manuever.

Performance Specifications

An integral part of the QFT approach to designing a control system is to embed the performance specifications in the design equations. The objective is to allow the designer to intelligently compare design choices with the effect on the performance specifications clearly displayed. QFT develops three types of specifications in the form of point-wise frequency bounds: stability bounds, tracking bounds, and disturbance bounds. The stability bounds define the region which can not be penetrated by the loop transmission function. The tracking and disturbance bounds are magnitude and frequency bounds on the Nichols chart which the loop transmission must not exceed if the specifications are to be met. Typically, the tracking bounds dominate in the low frequencies while the disturbance bounds dominate in the high frequencies. However, this thesis performs a digital QFT design and the sample rate places certain limits on the ability of the con-

troller to meet specific tracking and disturbance bounds. The design objectives are therefore redefined. The loop transmission function is designed to minimize the phase differential between the loop transmission and the stability bounds while maximizing the gain magnitude in the low frequencies. Professor Horowitz refers to this approach as maximizing the amount of loop transmission.

While performance specifications are not specifically incorporated into the loop shaping process, the tracking specifications are still used to design the prefilter. The tracking specifications for a fighter type aircraft are taken from previous theses which dealt with the AFTI F-16 and are in appendix D [2,25].

Conclusion

The linear equations of motion describing the CRCA across a range of simulated surface failures are developed. A weighting matrix is developed which converts the plant transfer function matrix (with a three-output C matrix) into a square 3x3 transfer function matrix.

III. The Discrete Plant Model

Introduction

This chapter describes the transformations of the plant equations required to design a digital controller for a continuous plant. Certain features are introduced when designing a control system for a sampled-data system which are not found in a continuous design. These unique aspects of the digital approach can be traced to implementing the control laws as difference equations in a computer and to introducing a sampler and zero order hold (ZOH) between the controller and the aircraft. The purpose of this chapter is to provide a brief overview of the fundamentals of a discrete control system, examine the necessary modifications to applying QFT in the digital domain, and the development of the discrete CRCA model.

Digital System Fundamentals

The z Plane A digital control system for a sampled-data system replaces the analog implementation of the controllers with a computer. Fundamental to the use of a computer as the controller for a continuous dynamic system is sampling. The plant outputs must be sampled to convert the plant response to a digital representation. At the same time, the digital output of the computer must be converted to a continuous signal which is then applied to the plant. Both processes affect how the design for a digital controller proceeds.

The sampling process converts a continuous signal into an impulse train. The value of the pulse at discrete intervals is given by

$$\mathcal{F}_d(kT) = \sum_{k=0}^{\infty} e(kT)\delta(t - kT) \tag{3.1}$$

where $\mathcal{F}_d(kT)$ is the discrete value of the continuous function $e(t)$ and $\delta(t - kT)$ is the unit impulse train. The Laplace transform of the expression in equation (3.1)

is given by

$$\mathcal{F}_d(s) = \sum_{k=0}^{\infty} e(kT)e^{-skT} \qquad (3.2)$$

which is the basis for the transformation which maps the complex variable s into the complex variable z by the relationship

$$z = e^{sT} \qquad (3.3)$$

Such a transformation is called the Z transform and is a mapping of a discrete time domain function into the complex variable z. The complex variable z is used in a representation of an infinite pulse train and can be formulated sometimes in a closed form or always in an open form. The closed form can be manipulated as a transfer function which lends itself to design work. The open form is used to implement the z transfer function in software as a series of recursive difference equations [20,23].

While the Z transform allows the tractable manipulation of a discrete pulse train, there are certain aspects of the z plane which are disadvantageous to the flight control system designer [24]. For instance, the imaginary axis of the s plane is mapped into the unit circle of the z plane. The poles of the plant tend to congregate near the unit circle boundary as the sampling time is decreased. The result is visibility into the degree of stability is lost. Also, numerical accuracy becomes important for any realistic sampling times; the difference between pole locations becomes extremely small as sample rates decrease. Therefore, numerical accuracy to the sixth or seventh place becomes important. In addition, the ς and w_n contours in the s plane become quite distorted in the z plane. Again, visibility into system performance is lost when the interpretation of such characteristics as damping or undamped natural frequency becomes difficult. Finally, there is no clear parallel in the z plane for such classical analysis tools as root locus or frequency response. Fortunately an alternative method exists which allows the analysis of a sampled data system which does not have these limitations.

The w/ Plane The w/ plane is the result of a bilinear transformation which maps the complex z variable into the complex w/ variable. Analogous to the complex s variable. the w/ variable has a real and imaginary part given by

$$w\prime = u + jv \qquad (3.4)$$

The interior of the unit circle is mapped into the left side of the familiar cartesian coordinate system. The exterior of the unit circle is mapped into the right side of the cartesian coordinate system. The w/ plane and the z plane are related by

$$w = \frac{2(z-1)}{T(z-1)}$$
$$z = \frac{-(w\prime - \frac{2}{T})}{(w\prime - \frac{2}{T})} \qquad (3.5)$$

The w/ plane is the same as the continuous s plane in form. The ς and w_n contours once again have the familiar shapes and techniques such as Bode analysis are applicable again. In other words, the w/ plane allows the control designer to analyze a sampled data system using the continuous domain techniques. However, there is no free lunch; certain features appear in the w/ plane which are not found in the s plane.

One feature of the w/ plane not found in the s plane is the dependance of root location on the sampling rate of the digital control system. As described by Professors Houpis and Lamont in *Digital Control Systems* [20], the correlation between the root location in the two planes is dependent on sample rates. The imaginary part of the root transforms accurately to the w/ plane if the product of the s plane imaginary part and half the sampling rate is equal to or less than 0.297. Similarly, if the square of the product of the s plane real part and half the sampling rate is much less than 2, the real part of the root shows good correlation in both planes. If either of the above conditions is not true, the root location is warped in the transformation process from the s to the z plane to the w/ plane. The degree of warping can be further increased by some of the approximations to

the s plane to z plane mapping. If the warping is too severe. the usefulness of the $w\prime$ plane approach to digital design is greatly reduced [20].

A second feature of the $w\prime$ plane is a result of the use of a zero order hold (ZOH). Continuous dynamic systems such as aircraft do not respond well when subjected to pulse inputs from the discrete output of a computer or sampler. Therefore, a ZOH is employed to convert the discrete signals into a continuous signal [20]. The largest frequencies present in the reconstructed signal must be roughly eight times less than the rate at which discrete signals are provided to the input of the ZOH in order to minimize jump discontinuities on the output of the ZOH at the sample instants. The ZOH must be considered part of the basic plant when the various transformations are performed. The result of a transformation from the s or z plane to the $w\prime$ plane is a right-half-plane zero whose value is given by

$$w\prime = \frac{2}{T} \tag{3.6}$$

A minimum phase plant in the s or z plane is therefore converted to a nonminimum phase plant in $w\prime$ plane. While a nonminimum phase plant is not inherently unstable the phase response of the plant will be radically different from a similar minimum phase plant. Consequently, as Professor Horowitz points out, the beneficial effects of feedback are reduced and the designer must therefore modify the expected performance from a nonminimum phase plant.

A final feature of the $w\prime$ plane is due the characteristics of the bilinear transformation. A unequal order numerator and denominator in the s plane is transformed through the z plane to an equal order numerator and denominator in the $w\prime$ plane. For instance, if a s plane numerator has only a gain term and the denominator has four poles in the s plane, the $w\prime$ plane numerator will gain four zeros: at least one right half plane zero, the sampling zero, and three other zeros, some of which may also be in the right half plane. The nonminimum phase zeros in addition to the sampling zero further complicate the design process by increas-

ing the severity of nonminimum phase characteristics. An equal order transfer function also has frequency characteristics which are different from the typical s plane transfer function. The magnitude of the $w\prime$ transfer function will approach a constant value rather than zero as the frequency increases. At the same time, the phase will approach zero degrees with increasing frequency (assuming positive gain and minimum phase). The frequencies at which the magnitude becomes constant and the phase goes to zero is a function of the sampling rate. These characteristics place limits on the performance improvements which can be achieved by feedback. Therefore, the performance limits are clearly related to the sampling rate.

Digital QFT The introduction of the nonminimum phase zeros by the transformation process does not prevent the application of QFT but it does require a certain modification of the loop shaping process. Because the nominal plant is nonminimum phase, the nominal loop must also be nonminimum phase. The right-half plane zeros can complicate the design of the nominal loop transfer function because the phase response characteristics are altered. An alternative to nonminimum phase loopshaping is made possible by the introduction of an all-pass- filter [21]. A function is initially defined as

$$F(w\prime) = \frac{1 - \frac{Tw\prime}{2}}{1 - \frac{Tw\prime}{2}} \tag{3.7}$$

which is just another expression for 1. The loop transfer function is rearranged so that the minimum phase part of the loop transfer function is cascaded with the nonminimum phase sampling zero.

$$L_{nmp} = (L_{mp}) \left(1 - \frac{Tw\prime}{2}\right) \tag{3.8}$$

where $1 - \frac{Tw\prime}{2}$ is the sampling zero.

The function in equation (3.7) is cascaded with the expression in equation (3.8) so that

$$(L_{nmp})(A(w\prime)) = (L_{mp}) \left(1 - \frac{Tw\prime}{2}\right) \left(\frac{1 + \frac{Tw\prime}{2}}{1 + \frac{Tw\prime}{2}}\right) \tag{3.9}$$

Frequency	Phase Shift
1 rad/sec	0.72 degrees
5 rad/sec	3.58 degrees
10 rad/sec	7.21 degrees
25 rad/sec	17.8 degrees
50 rad/sec	34.7 degrees
100 rad/sec	64.0 degrees
160 rad/sec	90.0 degrees
320 rad/sec	127 degrees

Table 3.1. Phase Shift due to $A(w\prime)$

The expression is rearranged to

$$L_{nmp} = (L_{mp}) \left(1 + \frac{Tw\prime}{2}\right) \left(\frac{1 - \frac{Tw\prime}{2}}{1 + \frac{Tw\prime}{2}}\right) \tag{3.10}$$

The QFT design is then developed based on the gain and phase characteristics of the minimum phase transfer function, L_{mp}, whose relationship to the orignal nonminimum phase transfer function is given by

$$L_{MP} = (L_{mp})(1 + \frac{Tw\prime}{2}) \tag{3.11}$$

The all-pass-filter, $A(w\prime)$, is given by

$$A(w\prime) = \frac{1 - \frac{Tw\prime}{2}}{1 + \frac{Tw\prime}{2}} \tag{3.12}$$

The magnitude of $A(w\prime)$ is unity over the frequency range but the phase response is given by

$$\Phi = 2 \arctan \left(\frac{\omega}{\omega_s}\right) \tag{3.13}$$

The phase shift given in equation (3.13) is no longer a part of the minimum phase nominal loop transfer function but mathematical validity requires that the phase shift be accounted for. Instead, the phase shift shows up in the frequency dependent stability bounds. Each boundary is shifted toward the zero degree phase point in accordance with the expression in equation (3.13). For the sample rate used in this thesis, the phase shift due to the all-pass-filter is given in Table 3.1. Examination

of Table 3.13 indicates very little phase shift occurs in the lower frequencies. Once the phase shift becomes significant, the boundaries have already folded into the UHFB. The straight boundary of the UHFB is shifted until it reaches 0 degrees.

The Hoffman Algorithm The conversion from the s plane to the $w\prime$ plane is performed using the Hoffman algorithm [9]. The algorithm does away with the intermediate results in the z plane and therefore avoids the numerical problems involved in z plane analysis. The approach solves the hyperbolic tangent function $\frac{AT}{2}^{-1} \tanh(\frac{AT}{2})$ with an infinite series solution. For this thesis, the series was truncated at the fourth term [1]. A simulation of the fourth order canard/flaperon actuators is performed in the s plane and the $w\prime$ plane. A simulation of the actuator model using MatrixX is performed first with a continuous step input. A second simulation with a continuous step input is performed after the actuator model is transformed to the $w\prime$ domain. The results are shown in Figure 3.1. Examination of the results shows identical responses are obtained in both planes indicating the dominant roots are not warped to any noticeable extent.

The Transformed Effective Plant

The nominal effective plant is obtained in the $w\prime$ plane by first converting the effective MIMO state space plant while still in the s plane into nine SISO transfer functions using the expression in equation (2.8). The actuator transfer function is cascaded with each effective plant transfer function. The cascaded transfer functions are then converted individually back into the state space format. The Hoffman algorithm is used to convert the nine s plane state space models into nine $w\prime$ state space models. Finally, the state space models are converted back into nine transfer functions which represent the nominal effective plant in the $w\prime$ plane.

Initially the fourth order actuators are cascaded with each transfer function before transformation to the $w\prime$ plane. However, nonminimum phase zeros in ad-
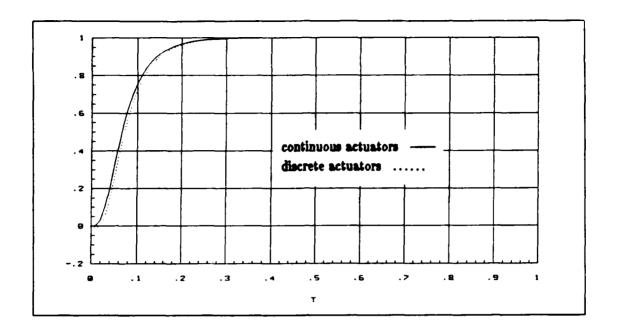
3-7

Figure 3.1. Step Response of Fourth Order Actuator in s and $w\prime$ Plane

dition to the sampling zero are introduced by the conversion process. While the nonminimum phase zeros in the individual elements of the transfer function matrix are not intrinsically detrimental, the right half plane roots of the determinant of the transfer function matrix should be limited to the sampling zeros in order to be considered minimum phase. In this case, the determinant of the effective plant had nine numerator roots consistently appearing in the right half plane: three at $w\prime = 160$, three at $w\prime = 289$, and three which varied around $w\prime = 1100$. The roots at $w\prime = 289$ and $w\prime = 1100$ are attributed to the fourth order actuators. The all-pass-filter could be modified for multiple zeros but the resultant phase shift on the stability boundaries would become too severe. Also, the roots at $w\prime = 1100$ varied by as much as 100 and would not be effectively cancelled by the all-pass-filter for all the members within the design set. Therefore, the fourth order actuators are replaced by a first order actuator which is given by

$$(57.3) \cdot \left(\frac{20}{s + 20} \right) \qquad (3.14)$$

The gain term premultiplying the transfer function is necessary to convert the

output of the model from radians to degrees. The control input matrix is in terms of degrees. The first order and fourth order actuators are simulated in the s plane. The results are shown in Figure 3.2. Examination of the results shows similar rise times but the first order response lacks the time lag of the fourth order actuators.
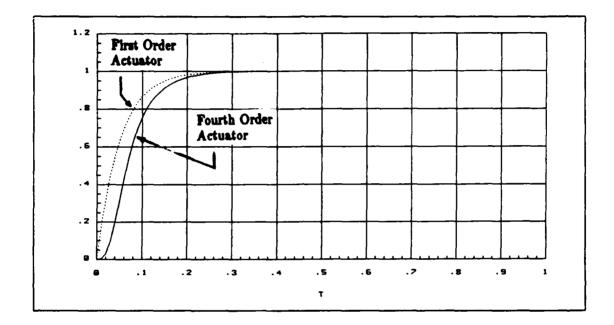

Figure 3.2. Step Response of Fourth vs First Order Actuator in s Plane

The first order actuators are cascaded with each transfer function in the effective plant matrix and individually transformed into the $w\prime$ plane. The determinant for all the effective plants in the design set is shown to be minimum phase excluding the nonminimum phase zeros due to sampling at $w = 160$ except cases 20, 22, and 24. These three cases have additional zeros and are therefore excluded from the design templates.

The Effective Plant in the $w\prime$ Plane The effective transfer function plant matrix in the $w\prime$ plane for the ACM entry nominal case is given in appendix A.

3-9

The q_{ij} Terms An important feature of a QFT MIMO design is the individual design of each feedback loop. In order to accomplish single loop design, the nxn MIMO plant is mapped into n^2 MISO plant equivalents. The following derivation is based on the desire to formulate a simple expression for the desired compensator [21]. The system control ratio, $T(w)$, which relates the vector of inputs to the vector of outputs is given by

$$T(w) = [I + PG(w)]^{-1} PG(w) \tag{3.15}$$

The control ratio for any single input-output pair is quite complex. However,if the expression is rearranged so that

$$\left[P^{-1} + G(w)\right] T(w) = G(w) \tag{3.16}$$

then only the inversion of the plant matrix is required. Since $P(w)$ is a matrix of transfer functions, the inverse $P(wl)$ is given by

$$P(w) = \frac{adj[P(w)]}{det[P(w)]} \tag{3.17}$$

The effective plant transfer functions are formed from the inverse of the individual terms of inverse of the plant and are referred to as the q_{ij} terms. The q_{ij} terms are derived by

$$q_{ij} = \frac{det[P(w)]}{adj(p_{ij})} \tag{3.18}$$

While simple to show, performing the necessary algebra to derive the q_{ij} can be tedious. However, the nominal plant for the ACM entry condition has several fortuitously placed zero terms which allows a general formulation of the q_{ij} terms to be derived. Once the general expression is derived, the individual q_{ij} terms are computed from the coefficients of the p_{ij} terms. The derivation is started with the effective plant matrix.

$$P_{eff} = \begin{bmatrix} a & 0 & 0 \\ 0 & b & c \\ 0 & d & e \end{bmatrix} \tag{3.19}$$

Where a. b. c. d. and e are the individual transfer functions of the effective plant matrix. The inverse of a square matrix is given by

$$P_{eff} = \frac{adj\,|P_{eff}|}{det\,|P_{eff}|}$$ (3.20)

The adjoint of P_{eff} is derived in general terms by

$$adj\,|P_{eff}| = \begin{bmatrix} be - dc & 0 & 0 \\ 0 & ae & -ac \\ 0 & -ad & ab \end{bmatrix}$$ (3.21)

The determinant of P_{eff} is

$$det\,|P_{eff}| = a(be - dc)$$ (3.22)

Therefore, using the expression in equation (3.18), the nominal q_{ij} terms are

$$Q_{eff} = \begin{bmatrix} a & \infty & \infty \\ \infty & \frac{be-dc}{e} & \frac{dc-be}{c} \\ \infty & \frac{dc-be}{d} & \frac{be-dc}{b} \end{bmatrix}$$ (3.23)

The nominal Q_{eff} is computed and the results are found in the appendix E.

Conclusion

The 3x3 effective plant in the s plane is transformed to the *w'* plane. The transformed plant matrix is shown to be minimum phase for 25 of the 28 possible cases in the design set for ACM entry and 17 of the 18 cases for TFTA. The templates which are used to determine the stability bounds are based on a reduced design set containing the 25 minimum phase plant transfer function matrices.

IV. Compensator and Prefilter Design

Introduction

The three compensators and three prefilters are designed using QFT. The first loop is picked on the basis of least uncertainty and the original method of QFT is used. The next two loops are designed using the improved method of QFT in order to reduce overdesign of the compensators. The compensators and prefilters designed in the w' plane are transformed to the z plane for implementation in the aircraft simulation.

Design of Pitch Rate Loop

Compensator One The first loop to be shaped is the pitch rate feedback loop. The decision which loop to design first is important because that loop compensator will exhibit the most overdesign. After the first loop compensator is designed, that compensator is incorporated into the nominal loop transmission function of the next two loops when the improved method of QFT is applied. Therefore, the decision which loop to shape first colors the remainder of the design. However, no consensus appears to exist on how to pick the first loop. Previous thesis efforts have started with both the most uncertain and the least uncertain transfer function set. Neither approach has been shown to be the optimal approach. For this thesis, based on advice from Professor Horowitz, the least uncertain transfer function set is picked as the first loop. The level of uncertainty is indicated by the size of the templates as determined by the phase angle and magnitude data for q_{ii}. In this case, the smallest templates and therefore least uncertain are obtained for q_{11}.

The compensator is developed by adjusting the frequency response of the loop transmission function (loop shaping) as depicted on the Nichols chart. The loop frequency response is adjusted by locating additional poles and zeros which

are cascaded with the unimpaired case. $q_{11}(w\prime)$. so that the frequency response of the loop at a particular frequency has the desired phase and gain characteristics. The process of loop shaping facilitates the point-wise tailoring of the frequency response of the compensator and plant as a whole unit. The transfer function used to start the loop shaping is called the nominal loop transmission nonminimum phase transfer function and is given by $L_1(w\prime)_{nmp} = q_{11}(w\prime)_{nmp}$. For the first loop, this function is

$$L_1(w\prime)_{nmp} = \frac{1.4981 \cdot 10^{-3} w\prime(w\prime + 0.00969)(w\prime - 1.07)(w\prime + 3723)(w\prime - 160)}{(w\prime - 19.9)(w\prime + 3.370)(w\prime - 1.649)(w\prime + 0.00402 \mp j0.03561)}$$
(4.1)

which is in the form of equation 3.8. The nominal loop transmission function is both unstable and nonminimum phase. Using an all-pass-filter, the nonminimum phase nominal transfer function is transformed to the minimum phase nominal case which is in the form of equation 3.10. The resulting transfer function used to begin the loop shaping process, $L_{1_{MP}} = q_{11}$, is given by

$$L_{1_{MP}} = \frac{1.4981 \cdot 10^{-3} w\prime(w\prime + 0.00969)(w\prime + 1.07)(w\prime + 3723)(w\prime + 160)}{(w\prime + 19.9)(w\prime + 3.370)(w\prime - 1.649)(w\prime + 0.00402 \pm j0.03561)}$$
(4.2)

Once a loop is shaped which meets the requirements, the compensator, $G_1(w\prime)$, is obtained by multiplying the loop transmission function by the inverse of the nominal transfer function.

The loop shaping is performed based on the stability bounds as determined by the templates for $q_{ii}(w\prime)$. The constant magnitude circle of 3 dB on the Nichols chart is picked as the absolute stability region which the loop transmission function can never penetrate. The 3 dB limit corresponds to a closed loop peak magnitude response for a step input of 1.41. The templates are translated but never rotated about the absolute stability region. The nominal plant is marked on the chart and the marks are connected to form the boundary for a particular frequency. At the low frequencies, the templates are sufficient to trace the boundaries because negligible phase shift is introduced by the all-pass-filter. At frequencies above 6

rad/sec, the phase shift becomes significant but at the same time, the templates have shrunk to a constant phase with a length equal to 12 dB. The stability boundaries therefore become overlapping vertical lines tangent to the constant magnitude circle in the minimum phase case. The resulting single boundary is called the universal high frequency boundary (UHFB). The UHFB is shifted toward the zero degree line on the Nichols chart with increasing frequency due to the effect of the all-pass-filter.

The loop transmission function must continually be to the right of the stability bound at each frequency and must be below the UHFB before the zero degree phase point is reached. The requirement to be below the UHFB at 0 degrees places a limit on the amount of loop transmission which can be achieved in the design. For the first loop of this design, the task is eased somewhat because the nominal point on the templates migrated to the top of the templates with increasing frequency. Therefore, the UHFB is above the constant magnitude circle and thus greatly eased the task of avoiding the UHFB in the higher frequencies.

The objective of loop shaping in a digital design is to maximize loop transmission magnitude while satisfying the boundary constraints at each frequency. Boundary constraints are satisfied by minimizing the phase difference between the loop transmission function and the stability boundaries. This approach maximizes system performance within the constraints due to sampling. The loop shaping is performed with the minimal number of poles and zeros possible in order to simplify the resulting compensator. Since this design is performed in the $w\prime$ plane, an equal number of poles and zeros must be added to $L_{1_{MP}}(w)$. The loop transmission gain is increased until the stability boundaries are just met in the higher frequencies. The result of maximizing the loop transmission is a high crossover point in the $w\prime$ plane. The loop transmission function is plotted in figure 4.1 and the data used to plot the loop transmission is found in appendix F.
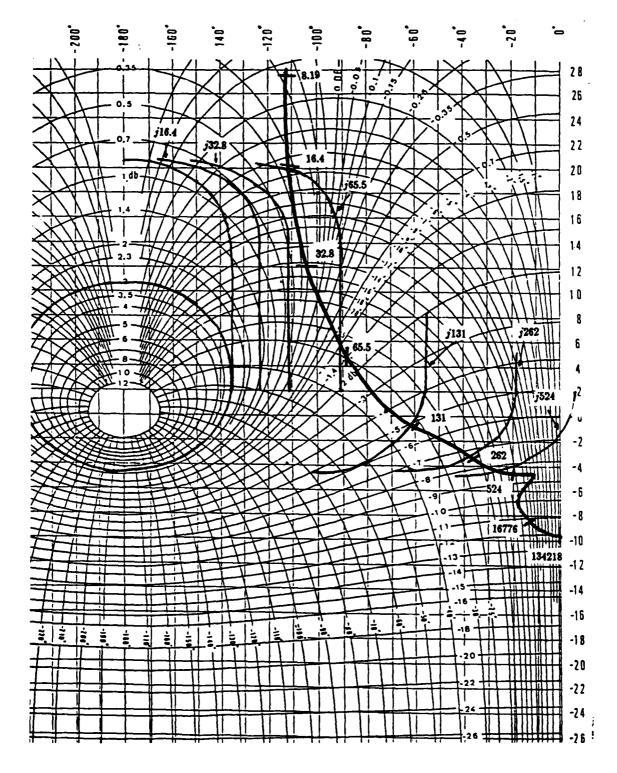
Figure 4.1. Loop Transmission Function for Pitch Rate Loop

Since the loop transmission function is equal to the minimum phase nominal plant multiplied by the compensator, division is performed to obtain the compensator. As an aside, the resulting compensator is only applicable to the minimum phase plant; however, the actual plant to be controlled is nonminimum phase. A polar plot analysis reveals a negative gain is required to maintain the necessary loop transmission characteristics for the nonminimum phase plant. Thus, for

$$L_{1_{MP}}(w\prime) = q_{11}(w\prime) \cdot G_1(w\prime) \tag{4.3}$$

the compensator for the minimum phase pitch rate loop is then given by

$$G_1(w\prime) = \frac{L_{1_{MP}}(w\prime)}{q_{11}} \tag{4.4}$$

After multiplication by a negative one to account for the effects of the all-pass-filter, the compensator for the nonminimum phase pitch rate loop is

$$G_1(w\prime) = -215.4 \frac{(w\prime + 0.005)(w\prime + 4.6)(w\prime + 44.5)(w\prime + 12000)}{(w\prime)(w\prime + 1.7)(w\prime + 5000)(w\prime + 5047)} \tag{4.5}$$

Prefilter One The purpose of the prefilter is to position the frequency response of the loop transmission function within the frequency bounds as described by the upper and lower tracking bounds. Since the compensator is designed to maximize the loop transmission, the closed loop time response to a step input without a prefilter is unrealistically fast. The prefilter is designed as a low pass filter which removes the higher order frequencies of the pilot command and therefore slows down the resulting closed loop system response. At the same time, the closed loop frequency response must remain within the bounds for the entire design set. Therefore, the worst case frequency responses for each impairment in the design set is used to form an upper and lower response boundary. The desired upper and lower tracking bounds are given in the form of transfer functions and are found in the appendix A. The prefilter is then used to position the closed loop responses of all the members of the design set within the desired response.

4-5

Deriving the frequency response of the closed loop transfer functions for the 25 transfer function of the design set is somewhat tedious so numerical methods are used instead. In general, the closed loop transfer function for a system with unity feedback without a prefilter is given by

$$T_i(w\prime) = \frac{G(w\prime)q_{ii}(w\prime)}{1 - G(w\prime)q_i(w\prime)}$$ (4.6)

where $T_i(w\prime)$ and $q_i(w\prime)$ are the closed loop transfer functions and corresponding open loop transfer functions, respectively, for the design set and $G(w\prime)$ is the compensator. The magnitude of the frequency response for each closed loop transfer function of the design set is found in decibels in terms of the open loop compensator and each plant in the design set as follows

$$T_i = 20 \log \left[\frac{G(jv)q_i(jv)}{1 + G(jv)q_i(jv)} \right]$$ (4.7)

$$T_i = 20 \log |G(jv)| + 20 \log |q_i(jv)| - 20 \log |1 + G(jv)q_i(jv)|$$ (4.8)

The last equation is solved repeatedly in a loop for each plant case and the maximum and minimum bounds for a discrete set of frequencies in the $w\prime$ plane are determined. The maximum upper case response is subtracted from the desired upper tracking bounds and the same operation is performed on the lower set of bounds. The result is a new set of bounds on $F(jv)$ which are used to develop the prefilter. The prefilter guarantees that the response of the entire design set is constrained within the desired tracking bounds. Therefore, the magnitude of the closed loop transfer function, $T(jv)$, cascaded with the is the prefilter, $F(jv)$, is given by

$$|T\prime(jv)| = |T(jv)||F(jv)|$$ (4.9)

Using the above approach, the prefilter for the first loop is given by

$$F_1(w\prime) = \frac{0.0005156(w\prime + 400)(w\prime - 160)}{(w\prime + 3)(w\prime + 11)}$$ (4.10)

Figure 4.2 displays the tracking response of the nominal closed loop response to a step input in the $w\prime$ plane. The nominal closed loop system consists of the

compensator and the $q_{11_{nmp}}(w\prime)$ with unity feedback and the prefilter on the input. This single input. single output simulation is performed as a quick check on both stability and tracking within the desired tracking boundaries and is not intended to replace a full-up simulation. As can be seen, the step response is within the desired upper and lower boundaries.
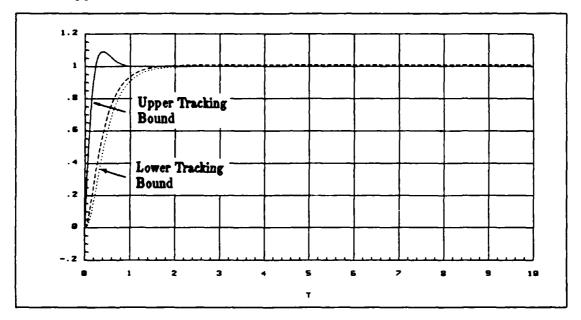

Figure 4.2. Closed Loop Step Response With Prefilter for Pitch Rate Loop

Design of Roll Rate Loop

   Compensator Two The second loop designed is the roll rate loop. The templates are generated using both the original method and the improved method. The original method develops the templates based on the frequency response of the q_{22} transfer function. The improved method develops the templates by incorporating information from the first loop design into the second loop using the following equations

$$L_{2_{eq}}(w\prime)_{nmp} = g_2 q_{22_e}(w\prime)_{nmp} \qquad (4.11)$$

$$L_{2_{eq}}(w\prime)_{nmp} = g_2 q_{22}(w\prime)_{nmp}\frac{1 + L_1}{1 + L_1 - \gamma} \qquad (4.12)$$

where

$$q_{22_c}(w\prime)_{nmp} = q_{22}(w\prime)_{nmp}\frac{1 + L_1}{1 + L_1 - \gamma} \tag{4.13}$$

and

$$\gamma = \frac{q_{11}q_{22}}{q_{12}q_{21}} \tag{4.14}$$

Comparison of the template data generated by q_{22} and q_{22_c} reveals some changes in template sizes in the lower frequencies but identical results in the higher frequencies. The conclusion drawn is since the linear aircraft model is inertially decoupled, there is little to be gained by using the improved method between the longitudinal pitch mode and lateral roll mode. However, the improved method templates are still used in this thesis for two reasons. First, the control surfaces are not decoupled; eight of the nine surfaces provide inputs to both the longitudinal and lateral modes. Second, inertial coupling is observed to occur for certain control surface failures.

The original $q_{22}(w\prime)_{nmp}$ transfer function is used as the nominal loop nonminimum phase transmission loop because γ is negligible throughout the frequency range for the nominal case. The $q_{22_{nmp}}$ transfer function is given by

$$L_2(w\prime)_{nmp} = \frac{1.0603 \cdot 10^{-3}w\prime(w\prime + 3489)(w\prime - 160)(w\prime + 0.0628 \pm j0.007)}{(w\prime - 19.9)(w\prime + 1.713)(w\prime - 0.0562)(w\prime + 0.1785 \pm j0.8124)} \tag{4.15}$$

The nominal transfer function is unstable and nonminimum phase. The all-pass-filter method is applied to nonminimum phase loop transmission. The resulting minimum phase transfer function, $q_{22} = L_{2_{MP}}$ used in the loop shaping process is given by

$$L_{2_{MP}} = \frac{1.0603 \cdot 10^{-3}w\prime(w\prime + 3489)(w\prime + 160)(w\prime + 0.0628 \pm j0.007)}{(w\prime + 19.9)(w\prime + 1.713)(w\prime - 0.0562)(w\prime + 0.1785 \pm j0.8124)} \tag{4.16}$$

The 3 dB constant magnitude circle is again used to define the absolute stability bounds. As in the first loop design, the roll rate loop is shaped to maximize low frequency gain within the constraints of meeting the high frequency stability boundaries in the $w\prime$ plane. The resultant high crossover value is similar to the first

loop transmission crossover. Dividing the final minimum phase loop transmission by the nominal loop, $L_{2_{MP}}(w)$, and changing the sign on the gain term to account for the all-pass-filter yields the following compensator for the nonminimum phase roll rate loop.

$$G_2(w\prime) = -252.1 \frac{(w\prime + 0.8)(w\prime + 7.09)(w\prime + 45.9)(w\prime + 749)(w\prime + 14000)}{(w\prime)(w\prime + 0.305)(w\prime + 1440)(w\prime + 2500)(w\prime + 8000)} \quad (4.17)$$

Prefilter Two Applying the same method used to design the first prefilter, the second set of prefilter bounds are determined. The resulting prefilter is given by

$$F_2(w\prime) = \frac{0.0001(w\prime + 500)(w\prime - 160)}{(w\prime + 2)(w\prime + 4)} \quad (4.18)$$

The closed loop step response for the compensator and $q_{22_{nmp}}(w\prime)$ is simulated similarly to the first loop design. The tracking step response is displayed in Figure 4.3 and is seen to be within the desired tracking upper and lower bounds.
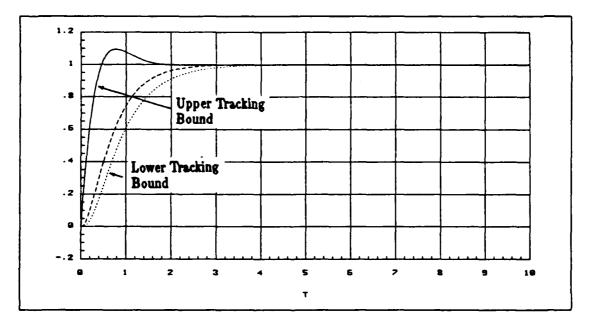
Figure 4.3. Closed Loop Step Response With Prefilter for Roll Rate Loop

Design of Yaw Rate Loop

Compensator Three The improved method of QFT is used to design the compensator for the last channel which controls the yaw rate variable. While there is no inertial coupling between the longitudinal and lateral modes for the unimpaired case, significant coupling exists between the two lateral modes. The inertial coupling is due to the off diagonal terms, $q_{23}(w\prime)$ and $q_{31}(w\prime)$, of the transfer function matrix. The templates are developed by modifying the $q_{33}(w\prime)_{nmp}$ term to incorporate the all-pass-filter and previous loop compensators into the transfer function. The expression for the effective $q_{33_e}(w\prime)_{nmp}$ is given by

$$q_{33_e}(w\prime)_{nmp} = \frac{q_{33}(w\prime)_{nmp}\varsigma}{\varsigma - \Lambda} \tag{4.19}$$

where

$$q_{33}(w\prime)_{nmp}(w\prime) = \frac{9.165 \cdot 10^{-4}w\prime(w\prime + 3757)(w\prime - 160)(w\prime + 0.0628 \pm j0.007)}{(w\prime - 19.9)(w\prime - 0.00125)(w\prime - 0.0562)(w\prime + 0.2763 \pm 1.89)} \tag{4.20}$$

$$\varsigma = (1 + L_1)(1 + L_2) - \gamma_{12} \tag{4.21}$$

$$\Lambda = \gamma_{23}(1 - L_1) - \gamma_{13}(1 + L2) - (\gamma_{12}u_2 + \gamma_{13}u_3) \tag{4.22}$$

However, due to the decoupling of the longitudinal and lateral modes, γ_{12} and γ_{13} are zero. After some algebraic manipulation, the expression for q_{33_e} is reduced to

$$q_{33_e}(w\prime)_{nmp} = \frac{q_{33}(w\prime)_{nmp}(1 + L_2)}{1 + L_2 - \gamma_{23}} \tag{4.23}$$

where

$$\gamma_{23} = \frac{(q_{22})(q_{33})}{(q_{23})(q_{32})} \tag{4.24}$$

After the algebraic manipulations are complete, the effective nonminimum phase nominal plant transfer function for q_{33} is given by

$$q_{33_e}(w\prime)_{nmp} = q_{33}(w\prime)_{nmp}\frac{(w\prime + 0.06268 \pm j0.00992)}{(w\prime + 0.0628 \pm j0.007)} \tag{4.25}$$

$$q_{33_e}(w\prime)_{nmp} = \frac{9.165 \cdot 10_{-4}\,w\prime(w\prime - 3757)(w\prime - 160)(w\prime - 0.06268 \pm j0.0992)}{(w\prime - 19.9)(w\prime - 0.00125)(w\prime - 0.0562)(w\prime - 0.2763 \pm 1.89)}$$

$$(4.26)$$

After modification by the all-pass-filter, the resulting nominal minimum phase loop transmission, $L_{3_{MP}}$, is used to develop the templates and start the final loop shaping. The loop is shaped as in the first two loops and the resulting compensator for the yaw rate channel is given by

$$G_3(u\prime) = -26.18\frac{(w\prime + 0.1)(w\prime + 2.45)(w\prime + 3.55)(w\prime + 30)}{(w\prime)(w\prime + 350)(w\prime + 0.025 \mp j0.0968)} \quad (4.27)$$

Prefilter Three Using the same upper and lower tracking response bounds as used for the roll rate channel, the prefilter for the third loop is developed using the same procedures as previously employed. The third prefilter is given by

$$F_3(w\prime) = \frac{0.001(w\prime + 500)(w\prime - 160)}{(w\prime + 2)(w\prime + 4)} \quad (4.28)$$

A single input single output simulation of the closed loop system is performed as in the previous two loops. The resulting step tracking response of the compensator with the nominial $q_{33_{nmp}}(w\prime)$ and the prefilter is shown in figure 4.4.

Transformation to the z Plane

While the design is performed in the $w\prime$ plane, the compensators and prefilters are implemented in the aircraft simulation in the z plane. The bilinear transformation is used to convert the transfer functions into the z plane. The relationship between the z and the $w\prime$ planes is given by

$$w\prime = \frac{2}{T}\frac{z - 1}{z + 1} \quad (4.29)$$

where T is the sampling time of 0.0125 sec.

4-11
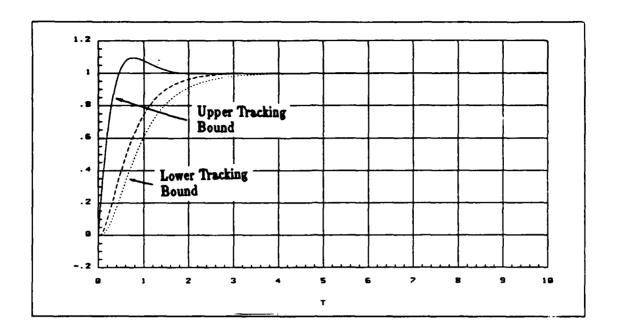
Figure 4.4. Closed Loop Step Response With Prefilter for Yaw Rate Loop

Using the bilinear conversion, the compensator for the pitch rate loop is given by

$$G_1(z) = \frac{-20.2983(z - 0.564792)(z + 0.973684)(z - 0.944107)(z - .999938)}{(z - 0.978973)(z - 0.937984)(z + 0.938544)(z - 1)}$$

(4.30)

The prefilter for the pitch rate loop is given by

$$F_1(z) = \frac{0.003315(z + 0.428571)}{(z - 0.871345)(z - 0.963190)}$$

(4.31)

The compensator for the roll rate loop is given by

$$G_2(z) = \frac{-20.1537(z - 0.554153)(z + 0.647963)(z + 0.977401)(z - 0.915136)(z - 0.990050)}{(z - 1)(z + 0.800000)(z + 0.879699)(z + 0.960784)(z - 0.996195)}$$

(4.32)

and the prefilter for the loop is given by

$$F_2(z) = \frac{0.000794941(z + 0.515152)}{(z - 0.951220)(z - 0.975309)}$$

(4.33)

The compensator for the yaw rate loop is given by

$$G_3(z) = \frac{-10.8538(z - 0.684211)(z - 0.969837)(z - 0.956588)(z - 0.998751)}{(z - 1)(z + 0.372549)(z - 0.999687 \pm j0.00120962)}$$

(4.34)

4-12

and the prefilter is

$$F_3(z) = \frac{0.000794941(z + 0.515152)}{(z - 0.951220)(z - 0.975309)} \tag{4.35}$$

Conclusion

Three rate controllers and associated prefilters are designed in the $w\prime$ plane. Each controller and prefilter is simulated with the nominal q_{ii} and is shown to have no overshoot and zero steady state error. The controllers and prefilters are transformed from the $w\prime$ plane to the z plane for implementation in the simulation.

V. Aircraft Simulation Setup and Results

Introduction

The QFT-designed digital FCS for the CRCA is simulated with the three pilot rate commands. Single and multiple pilot commands are simulated. The closed loop system is shown to be robust for the complete range of failures modeled by the reduced design set for ACM entry. Linearity of response is shown for a large range in magnitude of the command input. The TFTA condition is simulated with the pitch rate command but is found to be unsatisfactory. The first order actuator model is replaced with the fourth order model. Identical digital filters are cascaded with the digital controllers to account for the change in phase angle response of the loop transmission due to the additional poles of the fourth order actuators. The closed loop response is seen to be stable and almost equals the performance obtained with first order actuators in the longitudinal mode. The lateral mode exhibits a greater oscillatory behavior than previously obtained with the first order actuators. The output of the weighting matrix is examined for all nine control surfaces. The effects of saturation on the continued control surface cooperation are studied.

Simulation Setup

The CRCA is simulated using the nonlinear dynamic simulation capabilities of MatrixX. While the CRCA is simulated using the linear perturbation equations employed in the design process, the actuators are modeled to include deflection and rate limits which are not part of the design equations. The closed loop system is simulated as a sampled data system. The aircraft and actuators are modeled as continuous systems while the prefilters and controllers are modeled as discrete systems with a sample rate of 80 Hz. The sampler and ZOH are provided as part of the discrete block in the library of MatrixX simulation options. The block diagram

```
┌─────┐1   ┌─────┐2   ┌─────┐3
│ ONE │    │THREE│    │ SIX │
│SUPER│    │SUPER│    │SUPER│
│BLOCK│    │BLOCK│    │BLOCK│
│I:3 0:3│  │I:6 0:9│  │I:9 0:27│
└─────┘    └─────┘    └─────┘

                      ┌─────┐4
                      │PLANT│ 3
                      │STATE│
                      │SPACE│
                      │NS:8 │
                      │0:10 I:9│
                      └─────┘

Editing : SEVEN    (Continuous)
```
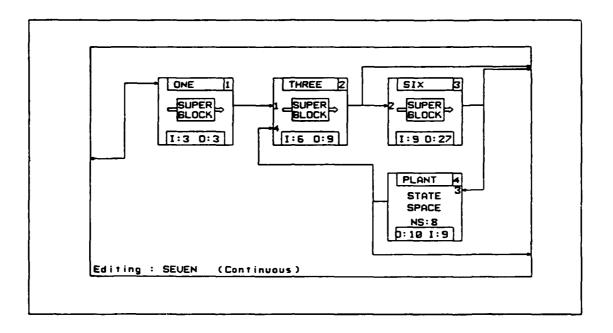
Figure 5.1. Simulation Setup

of the closed loop system is shown in Figure 5.1. Commands in the form of pulses are provided to the three inputs. The weighting matrix distributes the commands inputs to the nine actuators. All eight states, control deflections, control rates, and the generated states of longitudinal and lateral accelerations are provided as output.

The simulations for each command input are performed in a loop. The nominal aircraft is simulated and the resulting states, actuator deflections, and actuator rates are stored in a matrix. The nominal aircraft is replaced by an aircraft with simulated control surface damage (case 2 in appendix B) and the simulation is repeated. Similarly, the rest of the failure cases in the reduced design set for the ACM entry condition are sequentially simulated. The nominal CRCA for the TFTA condition is simulated but is found to be unsatisfactory. The unsatisfactory attempt to extend the design to the TFTA condition is discussed further in the next chapter.

Interpretation of the simulation results must be done while remembering that

the linear equations of motion are developed using perturbation methods. The linear equations of motion are developed with the assumption that the approximations $\sin x = x$ or $\cos x = 1$ are valid. If small angle assumptions are exceeded, the simulation results are not valid. Therefore, the initial transient state responses can be expected to closely reflect reality within the limits of the equations of motion. On the other hand, if a new trim condition is established at the completion of a command. the system response can not be expected to closely approximate reality. For instance. a simulation involving a pulse roll command leaves the aircraft in a banked orientation since the aircraft does not have a restoring moment which would otherwise reestablish the initial trim conditions. On the other hand, the aircraft tends to return to the initial trim conditions after the completion of a pulse pitch command and therefore the solutions to the equations of motion tend to remaim within the confines of the initial assumptions.

Actuators The control surface actuators are modeled using a deflection limiter and a limited integrator. In addition to acting as a rate limiter, the limited integrator also discontinues integrating whenever the rate limits are exceeded. When the actuator rates are no longer exceeded, the model immediately starts integrating again and therefore prevents a lag due to "integrator windup" in the actuator response. The values for the deflection and rate limits are given in Table 2.1.

Commands The simulated pilot commands are pitch rate, roll rate, and yaw rate. The commands are ramped to avoid saturating the actuator models. The commands reach full value or return to zero in 0.2 seconds.

Single Command Results

Each command is simulated twice with the reduced design set for the ACM entry condition. The simulation is performed first with a small magnitude command. The objective is to study the aircraft performance within a linear region

of response. The second simulation is performed using a large magnitude command. The purpose of simulating a command which saturates or nearly saturates the actuator models is to study the nonlinear response of the linearly designed control system. The left canard, left outer flap, left inner flap, left elevator, and rudder actuator deflection and rate responses are plotted once in the single input simulations to demonstrate typical deflections and velocities. The states which are plotted for each simulation run are pitch rate, roll rate, yaw rate, pitch angle, bank angle, sideslip, normal acceleration, and lateral acceleration. The results of simulating all the cases within the reduced design set are found in appendix G.

Pitch Rate Command for ACM Entry The first pitch rate command simulated is a 2 degree/second pitch command for three seconds. The command generates 1.96 g at the center of gravity (cg) of the aircraft. The response plots for all 25 cases can be found in Figure G.1 through Figure G.13 of appendix G. The surface deflections and rates are well within their limits. After the command, the surfaces are seen to return to their trimmed positions. The pitch rate state exhibits no overshoot and is seen to be identical for all aircraft in the reduced design set. The commanded pitch angle also exhibits no overshoot and is identical for all 25 cases in the reduced design set. The uncommanded rates are shown to be nearly zero and the associated angles are also virtually zero. The normal acceleration is shown to increase smoothly with no overshoot and builds to a full 1.9 g. Lateral acceleration is quite small. The results for simulating the unimpaired aircraft with the pitch rate command is shown in figures 5.2 and 5.3.

The pitch rate command is simulated for the second time with a magnitude of 12 degrees/second for three seconds. The command generates 6.8 g at the cg of the aircraft. The response plots for all 25 cases can be found in Figure G.14 through Figure G.21 of appendix G. No saturation is seen in any of the surfaces. The peak rate required to perform the command is 55 degrees/second and the largest deflection is 13 degrees. The commanded pitch rate state and associated pitch
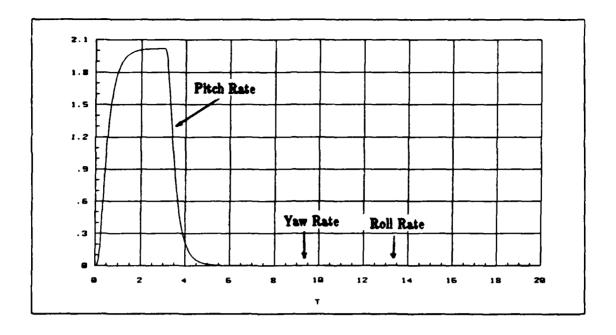
Figure 5.2. Pitch, Roll, and Yaw Rate Response for 2 DPS Pitch Rate Input

angle are identical for all 25 aircraft and no overshoot occurs. The uncommanded rates are shown to be virtually decoupled. Two damage cases are seen to maintain about 0.5 degree of sideslip after the initial transient while the remainder of the damage cases show virtually no sideslip. No bank angle is maintained in any of the cases after the transients die out. Normal acceleration increases smoothly but does not reach the full 6.8 g commanded. Negligible lateral acceleration is observed.

Roll Rate Command for ACM Entry The roll rate command is initially simulated with a 35 degree/second magnitude for 0.5 seconds. Surface position deflections and rates are seen to be well within limits except for three cases: 6,7 and 25. The exception cases demonstrate much larger surface movements and saturation is seen in the rudder for cases 6 and 7. The surfaces continue to deflect after the command is finished. Examination of the uncommanded states indicates a larger drift from the equilibrium position for cases 6 and 7 than for the rest of the cases. The commanded roll rate and bank angle are identical for all the cases simulated.

5-5
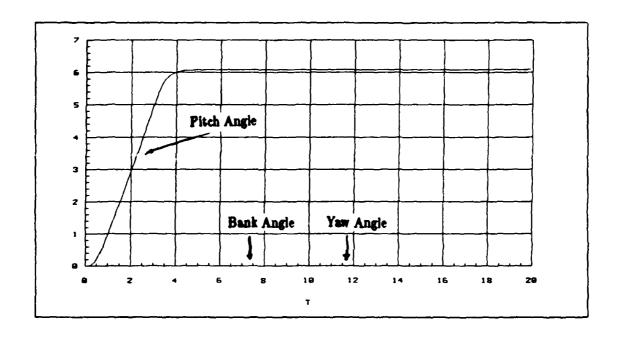
Figure 5.3. Pitch Angle, Bank Angle, and Sideslip for 2 DPS Pitch Rate Input

No overshoot is observed in the roll rate state or bank angle. Cross-coupling to the longitudinal pitch rate state is limited to less than 0.08 degrees/second for 24 of 25 cases. Coupling to the lateral yaw rate is limited to some transient behavior before being driven to zero. The response plots for all 25 cases can be found in Figure G.22 through Figure G.29 of appendix G.

The second roll rate command simulated is 135 degree/second for 0.5 seconds. *Extensive saturation is seen in all the control surfaces after the pulse command is complete.* Cases 6 and 7 are seen to diverge completely due to loss of control in the uncommanded states. The commanded roll rate and bank angle are identical for all cases for the first 10 seconds of the simulation. No overshoot is observed in pitch rate or bank angle. Cross-coupling is increased due to the loss of control of uncommanded states. The response plots for all 25 cases can be found in Figure G.30 through Figure G.37 of appendix G.

Yaw Rate Command for ACM Entry The yaw rate command is simulated with a magnitude of 1 degree/second for two seconds. The response plots for all 25 cases can be found in Figure G.38 through Figure G.45 of appendix G. The surfaces return to zero after the command, except for cases 6 and 7 which establish new equilibrium positions for all the surfaces of roughly 1 and 4 degrees from the initial trim position. The rates are minimal. Uncommanded states are negligible and return to zero. The commanded state is identical for all 25 cases but the degree of sideslip before returning to zero varies by roughly 0.5 degrees, except again for cases 6 and 7. These two cases establish a constant sideslip of about 2 degrees which is due to the new trim position of the surfaces.

The magnitude of the second yaw rate command is 5 degrees/seconds. The rudder saturates for case 7 and nearly saturates for case 6. All rates are driven to zero except case 7 which starts a divergence at 12 seconds into the simulation. The uncommanded states display an increased transient response than seen previously for the small magnitude input. Eventually, the uncommanded states then return to zero for almost all the cases. The commanded yaw rate is identical for all simulations. The response plots for all 25 cases can be found in Figure G.46 through Figure G.53 of appendix G.

Pitch Rate Command for TFTA The entire set of single input commands was to be simulated for the TFTA condition. However, upon examination of the nominal CRCA response to a 2 degree/second command, further simulations are not performed. The control surfaces displayed a high frequency flutter with a small magnitude. The pitch rate response in figure 5.4 exhibits a high frequency mode overlaid on the nominal response which severely distorts the response. However, the pitch angle response is quite similar to that achieved in the ACM entry simulation. The uncommanded roll and yaw rate are extremely small but appear to diverge after 18 seconds of simulation.
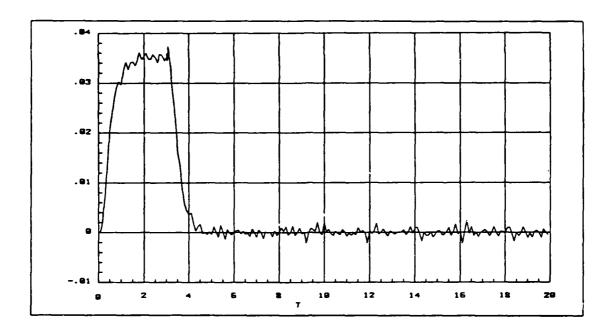
Figure 5.4. Pitch Rate Response of Nominal CRCA for TFTA Condition

Conclusion of Single Command Input Simulations The objective of the single input commands is to demonstrate decoupling and transient response. Overall, the degree of cross-coupling is shown to be quite small for all aircraft within the reduced design set for ACM entry. In addition, no overshoot or oscillation is seen in a commanded rate state or associated angle. The longitudinal mode is shown to be the most robust to surface failures which included 100/effectiveness of the left canard. The pitch rate state is seen to have the fastest rise time while the two lateral rate states are slightly slower. Minimal lateral acceleration is seen for a longitudinal command. However, lateral commands develop a sizeable amount of longitudinal acceleration. The negative longitudinal acceleration for the pulse roll command can be partially attributed to the lack of thrust modeling in the equations of motion. With the aircraft in a banked orientation and no thrust, generation of lift is reduced, vertical velocity increases, and hence the negative acceleration.

During the roll simulations, the control surfaces did not return to their equi-

5-8

librium positions upon completion of the pulse command. While the rates went to zero, the surface position deflections continued. As a result, the uncommanded states such as sideslip are seen to slowly increase. The drift after the command is complete is attributed to the use of rates as the controlled states. In all cases, the rates are driven to zero after the command. However, once the rates are driven to zero, the control system can no longer regulate the associated angles. As a consequence, the control surfaces begin to drift in response to the dynamics of a nontrimmed orientation.

Simulations for the TFTA condition are not performed. The constant gain FCS which is designed for aerodynamic conditions of 0.9 Mach and 30000 feet is unstable for aerodynamic conditions of 0.9 Mach and 200 ft.

Coordinated Turn

A coordinated turn for the ACM manuever is simulated by a pulse roll command of 74.5 degrees/second for 0.5 seconds, a step pitch rate command of 1.46 degrees/second, and a step yaw rate command of 1.46 degrees/second. The response plots for all 25 cases can be found in Figure G.54 through Figure G.61 of appendix G. All the commands are ramped as in the previous simulations. For most of the cases, the control surfaces move rapidly but well within tolerances during the duration of the pulse roll command. The surfaces start to drift after the pulse roll command as observed in the earlier single command simulations for roll or yaw rates. Cases 6,7, and to a smaller extent case 25 display the most drift. All control surface rates are driven uniformly to zero except the rudder: several damage cases exhibited roughly a 0.5 degrees/second rate in the steady state. The three commanded rates are uniform for all members in the design set. The bank angle and pitch angle are indistinguishable for all aircraft within the reduced design set. However, a greater range of sideslip is seen with an average of about 2 degrees for all cases except cases 6 and 7.

5-9

Fourth Order Actuators

The first order actuators are replaced by the fourth order actuators given in equation 2.9. Without any changes in the digital controllers, the closed loop system is unstable. A digital filter is developed which is cascaded with each controller. The numerator of the filter is the z plane mapping of the three new poles introduced by the fourth order actuators. The denominator consists of three nondominant poles. The resulting filter is given by

$$F(z) = \frac{0.39(z - 0.42667 \pm 0.29457)(z - 0.23841)}{(z - 0.5)^3} \tag{5.1}$$

The purpose of the digital filter is to restore the original loop transmission characteristics by cancelling the three new s plane poles of the fourth order actuator with the three z plane zeros. The three nondominant poles do not add any phase or magnitude information in the frequency range of interest. If the original loop transmission characteristics are restored, system performance similar to the original system with first order actuators is expected.

The first simulation is performed with a six degrees/second pulse command for three seconds. The magnitudes of the surface deflections and rates for the pitch rate simulation are roughly proportional to that obtained with 2 degree/second pitch command with first order actuators. However, the three damage cases simulating 25%, 50%, and 100% left canard loss exhibit a damped oscillatory motion of the control surfaces not seen in the earlier simulations. In addition, the states exhibit a larger variation in responses between the bracketing cases. Where the simulations with first order actuators display identical pitch rate state responses for all 25 cases, the fourth order actuators simulation produce state responses which do not track the pulse command well in several cases. In addition, where the unmodified simulations produced a 2 degrees/second response for a 2 degrees/second command, the modified actuators produced roughly 8 degrees/second for a 6 degrees/second command. Attempts to further limit the error by varying the gain

on the digital filter resulted in an unstable system. Uncommanded rate states and associated angles are maintained near zero but their transient behavior is much more oscillatory than seen in the earlier unmodified simulation. The response plots for all 25 cases can be found in Figure G.62 through Figure G.69 of appendix G.

A second simulation is performed with a 90 degrees/second pulse pitch command for 0.5 seconds. The surface deflections show a damped oscillatory behavior which is similar to the responses achieved with a first order actuator. Cases 6,7, and 25 again display large surface movements but with an oscillatory mode overlaid on the surface excursion. All surface rates are driven to zero after a series of medium damped oscillation except for two rudder cases. The rudder for cases 6 and 7 saturates much quicker than in the first order actuator simulations. The roll rate responses display some oscillation after the command but are maintained at zero. The response plots for all 25 cases can be found in Figure G.70 through Figure G.77 of appendix G.

Overall, better system response is obtained in the longitudinal mode than in the lateral mode with the fourth order actuators. In neither case can the loop transmission be said to be completely restored. Oscillatory behavior is seen in the surface deflections, rates, and the states which is not present in the earlier simulations. The lateral mode oscillations are of a higher frequency than the longitudinal mode oscillations. The oscillation is seen in almost all the lateral states. In most cases, the commanded state responses of pitch rate and roll rate are seen to be quite similar to their responses obtained with first order actuators.

Examination of Weighting Matrix Output

A final simulation is performed to examine the individual components which form the pitch rate output. Two cases are examined: the nominal case and and the 100% canard failure case using both first order and fourth order actuators. Examination of the transfer functions found in appendix C reveals that the pitch rate

5-11

state can be viewed as the composite of the outputs of the eight open loop transfer functions (with the appropriate feedback). Each transfer function represents a portion of the total system response. The weighting matrix is used to convert a single input into eight inputs with different relative authorities. The weighting matrix outputs, via the actuator models, are then the inputs to the eight transfer functions which make up the pitch rate output. The objective of the weighting matrix is to maximize the degree to which the surfaces, and therefore the control inputs to the plant, work together. If the control surfaces work against each other, then greater surface deflections will be necessary to implement a particular command. A study of the individual component outputs is an indication of the degree the control surfaces begin to fight each other under simulated failure conditions.

Examination of the outputs of the eight pitch rate transfer functions by themselves is not possible since each has an unstable pole. Therefore, an alternative method is devised. The time histories of the outputs of the eight actuators are obtained for a 2 degree/second pitch rate command. The actuator outputs are taken because the weighting matrix outputs undergo an integration by the actuators before going to the plant. Each time history is multiplied by the its corresponding value in the third row of the input B matrix from chapter two; first time history multiplied by the $B(3,1)$ term, second by $B(3,2)$, and so on. The time histories are obtained for the healthy aircraft and the 100% canard loss as are the corresponding input matrices for the two cases. The results are plotted in terms of symmetrical control surfaces and can be found in Figures 5.5 through 5.7.

The results of the simulation are not unexpected in the healthy aircraft. The symmetrical surfaces exert equal amounts of effort and work together. The failure case is seen to display unequal efforts in terms of the magnitude of the control surface motions. For the failure case, the canards displayed slightly different responses but all six trailing flaps displayed different levels of response. However, no surfaces are seen to work against each other by moving in opposite directions.

The first order actuators are replaced by fourth order actuators. Examination of the nominal aircraft again shows the surfaces working together and with equal effort. The failure case clear displays conflicting control inputs from symmetrical surfaces. Opposing inputs from symmetrical control surfaces will generate a rolling and/or yawing moment which might account for some of the inertial cross-coupling observed for failure cases. As an aside, the conflicting surface movement is not seen for all surface failure cases; a simulation run with a 100% outer flap loss did not manifest any conflicting surface inputs.

LEFT AND RIGHT CANARD

LEFT AND RIGHT ELEVATORS

LEFT AND RIGHT INNER AND OUTER FLAP
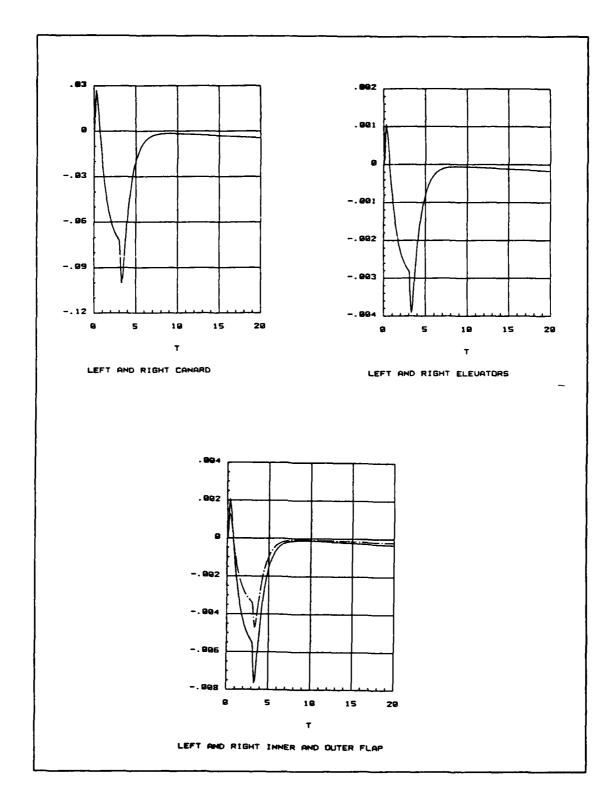
Figure 5.5. Control Inputs for Unimpaired CRCA With First Order Actuators
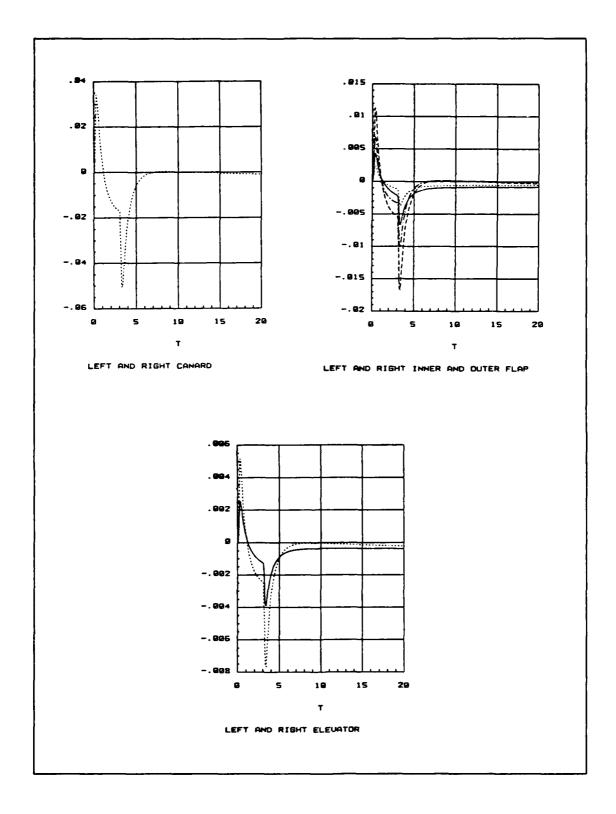
Figure 5.6. Control Inputs for CRCA With 100% Left Canard Loss and First Order
Actuators
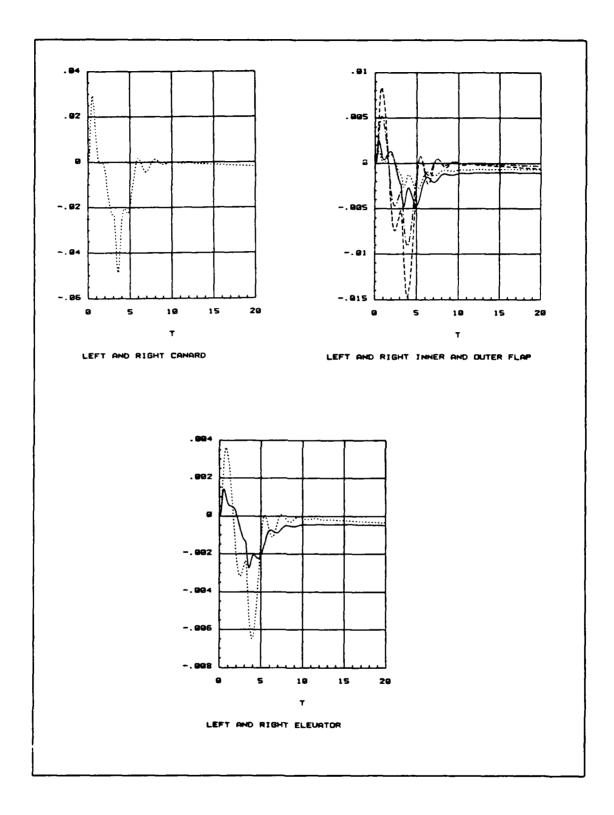
Figure 5.7. Control Inputs for CRCA with 100% Left Canard Loss and Fourth Order Actuators

5-16

Conclusion

   The closed loop aircraft is simulated with a variety of inputs. Cross-coupling between lateral and longitudinal states is seen to be held to a minimum. Coupling between the lateral states for a lateral command is somewhat larger in some failure cases. The objective of reducing overshoot in pitch rate is obtained with first order actuators. The method of substituting of fourth order actuators into a system designed for first order actuators does not prove to be wholly satisfactory. Restoration of the loop transmission characteristics is not complete. Given sufficient time. improvement of the loop characterstics may be possible with improved pole locations in the digital filter. Examination of the weighting matrix outputs reveals conflicting control inputs for at least one failure case.

VI. Conclusions and Recommendations

Conclusions

The application of QFT to a sampled data system is shown to be successful. The aircraft FCS continues meeting performance objectives in spite of control surface damage in the simulations. Pitch overshoot is nonexistent for a pitch rate command and minimal inertial cross- coupling occurs for the aircraft within the reduced design set. Damped oscillations are not observed in any of the controlled variables or associated angles. Once the weighting matrix is derived, the design process is highly transparent with the trade-offs clearly detailed. The surface deflections are seen in the simulations to be minimal. The design is tolerant to control surface failures. In conclusion, the use of QFT to design a FCS for an unstable, nonminimum phase aircraft is effective for the conditions upon which the design is based.

However, extensions to conditions other than the design conditions such as the TFTA aerodynamic condition or the use of fourth order actuators is not as successful. The use of the fourth order actuators does not have a large impact on the response of longitudinal mode states to a pitch rate command. However, the lateral mode responses to a roll rate command are divergent for several failure cases. The design is unacceptable for direct application to the TFTA condition. The lack of success in extending the design beyond the original conditions only emphasizes the need to incorporate such information into the design process from the beginning.

The following discussions highlight some of the issues raised during the design process.

Weighting Matrix Different values other than zero are originally used in the off-diagonal terms of the left hand side of equation (2.12). The objective is to

mirror physical reality in that complete decoupling between states is not possible. However, this approach is discarded because the terms of the resulting weighting matrix no longer made physical sense. The magnitudes of terms in the weighting matrix for symmetrical surfaces such as left and right canard are found to be unequal. Different weightings for similar surfaces would lead to an untrimmed aircraft. As the off-diagonal terms of the left hand side of equation (2.12) decrease in magnitude, the difference between symmetrical terms of the weighting matrix become smaller. Zeros are therefore used in the off-diagonal terms and the resulting weighting matrix is symmetrical with respect to like surfaces.

While the weighting matrix is developed in the continuous plane, the minimum phase properties of the effective plant are verified in the discrete $w/$ plane. As an intermediate step in the conversion from the continuous to the discrete domain, the effective plant is modified by cascading the actuator model with each transfer function in the plant matrix. When the determinant of the effective plant is examined in the s plane without cascading the actuator model, additional cases of nonminimum phase plant matrices are found. The correlation between the weighting matrix and when best to determine whether the plant is minimum phase or not is not clear. Further study is needed to determine if the test for an adequate weighting matrix should be performed in the continuous or discrete domain and with or without the actuators cascaded with the basic plant.

The use of the weighting matrix, while not truly a part of QFT, is imposed by the requirements of QFT. The method used to develop the terms of the weighting matrix appears satisfactory. However, there is no indication at the onset of the design process if the weighting matrix derived in this thesis is the optimal weighting matrix for the CRCA. The examination of the component responses of pitch rate output reveals under some failure conditions the surfaces are fighting each other. Obviously, optimal performance under failure conditions can not be achieved if the control inputs are not compatible with each other. The full benefits of QFT may

not be realized on nonsquare plants if the weighting matrix is developed without some indications on how to minimize the amount of crossed control inputs.

TFTA The control system designed for the ACM entry condition could not be extended to include the TFTA condition without some type of gain scheduling. The difference between the two conditions is the relative aerodynamic pressure. The design philosophy applied in this thesis is to maximize the loop transmission. Therefore, the design is optimized for the aerodynamic conditions represented by ACM entry. A possible approach to extending the design to TFTA would be to reduce the loop transmission. Examination of the loop transmission plot similar to the one in Figure 4.1 reveals the upper and lower limits on the allowable gain adjustments before the stability boundaries are violated. The probable tradeoff would be to sacrifice performance at the ACM entry condition while increasing performance in the TFTA condition.

Fourth Order Actuators The QFT design is based upon the cascade combination of the effective plant and the first order actuators. After the z plane controller is implemented, a simulation is performed using fourth order actuators without changing the controller. The replacement causes the system to become unstable. The two actuator models have very similar step responses in the time domain which would initially indicate the two models could be interchanged. An explanation for the unstable response lies in the frequency domain. The phase response of the two models is quite different. The first order model contributes a maximum of -90 degrees of phase angle while the fourth order model will contribute up to -360 degrees. The difference in phase angle is critical when one considers that the loop transmission is shaped based on a desired loop phase response. Therefore, any changes in the phase response will obviously have a dramatic effect in the regions where the stability boundaries are rigorously satisfied.

The use of the digital filter with the fourth order actuators almost restores

the loop transmission characteristics of the system with first order actuators. The system performance for a pitch rate command is quite similar to that achieved with the first order actuators except for the increased magnitude of the commanded state and the oscillatory behavior of the states and control surfaces. The response of the aircraft for the roll rate command is not satisfactory. Several failure cases diverged with fourth order actuators that are stable with the first order actuators. One conclusion drawn is the use of first order actuators obscures information which is then unaccounted for in the design. The poor performance of the roll rate command simulation indicates the unaccounted information is critical and needs to be built into the design.

The gain on the filter is originally such that the steady state error of the filter is zero. However. the closed loop system is unstable so the gain is varied until the desired performance is obtained. The best performance is obtained with the gain equal to 0.39; a lower value caused the magnitude of the response to increase dramatically while a larger gain value induced oscillation and eventually instability.

The approach of designing with first order actuators and simulating with fourth order actuators is imperfect at this stage. Insufficient time remained to fully explore alternative pole postions or gains. The use of the filter in the discrete domain to cancel the poles of the actuators in the continuous domain has the unintended effect of amplifying the command response. In addition, the oscillatory behavior due to the set of complex poles in the fourth order actuators is not adequately controlled especially in the lateral mode. On the positive side, the technique does allow the designer to study the overall system behavior with higher order actuators. In the case of this thesis, the increased oscillatory behavior seen with the higher order actuators indicates a shortcoming of designing with simplified actuators. Such results only further stress the need to develop techniques which incorporate the higher order actuators into the plant model before the loop shaping

is performed.

Digital Aspects The use of the $w\prime$ plane to carry out the design appears to be an excellent alternative to designing in the z plane. The use of the Hoffman algorithm allows the equations of motion to be transformed from the s plane to the $w\prime$ plane without manipulating the intermediate results in the z plane. Once in the $w\prime$. the loop transmission function is shaped based on Professor Horowitz's repeated exhortations to "pack in as much loop transmission as possible". The reason behind this approach is based on the inherent limitation of sampling. However, this approach results in a high open loop bandwidth in the vicinity of 100 rad/sec in the $w\prime$ plane. Time did not permit a study of the correlation between a high open loop bandwidth in the $w\prime$ plane and the actual bandwidth in the z plane. With the increasing use of digital flight control systems, an investigation into the frequency relationships of the s, z, and $w\prime$ is warranted.

Recommendations

1. A digital QFT control system with a sample rate of 80 Hz for the CRCA should be performed with tracking and/or disturbance bounds. The stability bounds in this thesis are easily satisfied and therefore the further constraint of tracking and/or disturbance bounds should be within reason. Once the design is complete, further thesis efforts should be directed at fully characterizing the design. Susceptibility to noise inputs from the sensors or in terms of wind gusts and man-in-the-loop simulations are examples of areas of possible exploration. The objective is to demonstrate the qualitative aspects of a QFT based flight control system.

2. The use of the CRCA equations of motion provide an excellent opportunity for further thesis efforts regardless of technique applied. The aircraft is representative of an advanced airframe with its attendant problems of insta-

bilities and nonminimum phase characteristics. If flight control research at AFIT is to continue to be relevant to outside agencies, research efforts should concentrate on the types of problems presented by the CRCA.

3. The software package MatrixX is an excellent method to simulate dynamic systems. However, there are limits to its usefulness as a design package due to numerical problems. Limitations exist within MatrixX on the number of variables which can be used, the accuracy available in the manipulations of complex numbers, the maximum order of polynomials which can be handled, and reliability with which phase angles are calculated for unstable or non-minimum phase systems. The numerical limitations of MatrixX need to be understood and disseminated to future AFIT students.

4. The development of the terms within the weighting matrix need to be corre-lated with some measure of optimality. Until the weighting matrix is shown to be optimal, the full benefits of QFT on nonsquare plants may not be re-alized. For instance, an optimal weighting matrix may eliminate the small amount of sideslip observed for the two failure cases which differed markedly from the other 23 cases in the pitch rate simulations. Examination of the individual component responses for a particular output reveals at least part of the unwanted inertial cross-coupling may be due to control surfaces work-ing against each other. The weighting matrix for this thesis is developed based on the healthy aircraft. An alternative approach might be to develop the weighting matrix based on the worst case aircraft. Another possibility is to average the terms of several weighting matrices developed for several different types of failures to produce a composite weighting matrix.

5. The states used for feedback in this thesis are pitch rate, roll rate, and yaw rate. Once the rates are driven to zero, control over the associated angles is lost. The situation is especially exaggerated in the rolling mode since an intrinsic restoring moment does not exist. The conclusion drawn is the use

6-6

of only rates is not a satisfactory set of feedback states. A better set might be pitch rate, roll rate, and sideslip.

6. The relationship between higher order actuators and nonminimum phase zeros in the discrete domain should be investigated. Techniques need to be developed that allow the incorporation of higher order actuators into the basic plant before loop shaping is accomplished. As part of this investigation, the restoration of the loop transmission characteristics through the use of the digital filter should be further explored.

Appendix A. *Tracking Response Models*

The tracking response models are taken from previous theses which dealt with a QFT design for the AFTI F16. The response models are given first for the continuous case and then for the $w\prime$ case. The $w\prime$ versions are obtained by using the Hoffman algorithm to transform from the s plane through the z plane to the $w\prime$ plane. The sample rate is 80 Hz.

Roll Rate Model

Upper Bound

$$T_u(s) = \frac{2.136(s - 1.3)}{s^2 + 2.667s - 2.776}$$

$$T_u(w\prime) = \frac{-0.0133(w^2\prime - 158.7w\prime - 208)}{w^2\prime - 2.667w\prime + 2.776)}$$

Lower Bound

$$T_l(s) = \frac{6.937}{(s + 0.75)(s + 2.5)(s + 3.7)}$$

$$T_l(w\prime) = \frac{5.642 \cdot 10^{-7}(w - 160)(w - 280.7)(w - 273.7)}{(w + 3.699)(w + 2.5)(w - 0.75)}$$

Pitch Rate Model

Upper Bound

$$T_u(s) = \frac{4.167(s + 2.667)}{s^2 + 5.334s + 11.113}$$

$$T_u(w\prime) = \frac{-2.604 \cdot 10^{-2}(w - 160)(w + 2.667)}{(w + 2.667 \pm j2.0)}$$

Lower Bound

$$T_l(s) = \frac{63.75}{(s + 1.5)(s + 4.25)(s + 10)}$$

$$T_u(w\prime) = \frac{5.173 \cdot 10^{-6}(w - 160)(w - 269.5)(w - 285.3)}{(w + 9.987)(w + 4.249)(w + 1.5)}$$

Yaw Rate Model

Upper Model

$$T_u(s) = \frac{4.167(s + 2.667)}{s^2 - 5.334s + 11.113}$$

$$T_u(w\prime) = \frac{-2.604 \cdot 10^{-2}(w - 160)(w + 2.667)}{(w + 2.667 \pm j2.0)}$$

Lower Model

$$T_l(s) = \frac{63.75}{(s + 1.5)(s + 4.25)(s + 10)}$$

$$T_u(w\prime) = \frac{5.173 \cdot 10^{-6}(w - 160)(w - 269.5)(w - 285.3)}{(w + 9.987)(w + 4.249)(w + 1.5)}$$

Appendix B. *Control Surface Failure List*

Case	Failure Description for ACM Entry
1	unimpaired aircraft
2	25% rudder loss
3	50% rudder loss
4	100% rudder loss
5	25% outer flap loss
6	50% outer flap loss
7	100% outer flap loss
8	25% inner flap loss
9	50% inner flap loss
10	100% inner flap loss
11	25% outer flap and 25% elevator loss
12	50% outer flap and 50% elevator loss
13	100% outer flap and 100% elevator loss
14	25% elevator loss
15	50% elevator loss
16	100% elevator loss
17	elevator fail to trail
18	canard locked at 5 degrees
19	rudder fail to trail
20	canard fail to trail
21	outer flap fail to trail
22	inner flap fail to trail
23	canard and rudder fail to trail
24	canard and outer flap fail to trail
25	outer flap and elevator fail to trail
26	25% canard loss
27	50% canard loss
28	100% canard loss

The reduced design set for ACM entry consists of cases 1 to 19,21,23,25 to 28.

Case	Failure Case List for TFTA
1	unimpaired aircraft
2	canard and outer flap fail to trail
3	rudder fail to trail
4	outer flap fail to trail
5	canard fail to trail
6	25% outer flap loss
7	50% outer flap loss
8	100% outer flap loss
9	25% outer flap and 25% elevator loss
10	50% outer flap and 50% elevator loss
11	100% outer flap and 100% elevator loss
12	outer flap and elevator fail to trail
13	25% rudder loss
14	50% rudder loss
15	100% rudder loss
16	25% canard loss
17	50% canard loss
18	100% canard loss

Appendix C. *Plant Open Loop Transfer Functions for Nominal ACM Case in the s Plane*

Actuator dynamics are not included in the following transfer functions.

Pitch Rate Transfer Functions

$$p11 = \frac{0.102s(s - 1.035)(s - 0.0096)}{(s - 1.694)(s + 3.37)(s - 0.00402 \pm j0.0356)}$$

$$p12 = \frac{0.102s(s - 1.035)(s - 0.0096)}{(s - 1.694)(s + 3.37)(s - 0.00402 \pm j0.0356)}$$

$$p13 = \frac{-0.028s(s + 1.296)(s + 0.0102)}{(s - 1.694)(s + 3.37)(s + 0.00402 \pm j0.0356)}$$

$$p14 = \frac{-0.022s(s + 1.253)(s + 0.0101)}{(s - 1.694)(s + 3.37)(s + 0.00402 \pm j0.0356)}$$

$$p15 = \frac{-0.028s(s - 1.296)(s - 0.0102)}{(s - 1.694)(s - 3.37)(s - 0.00402 \pm j0.0356)}$$

$$p16 = \frac{-0.022s(s - 1.253)(s - 0.0101)}{(s - 1.694)(s - 3.37)(s + 0.00402 \pm j0.0356)}$$

$$p17 = \frac{-0.02s(s + 1.312)(s + 0.0102)}{(s - 1.694)(s + 3.37)(s + 0.00402 \pm j0.0356)}$$

$$p18 = \frac{-0.02s(s + 1.312)(s + 0.0102)}{(s - 1.694)(s + 3.37)(s - 0.00402 \pm j0.0356)}$$

$$p19 = 0$$

Roll Rate Transfer Functions

$$p21 = \frac{0.076(s - 0.00126)(s - 0.4247 \pm j4.505)}{(s + 2.017)(s + 0.0562)(s + 2.492 \pm j1.834)}$$

$$p22 = \frac{-0.076(s - 0.00126)(s - 0.4247 \pm j4.505)}{(s - 2.017)(s - 0.0562)(s - 2.492 \pm j1.834)}$$

$$p23 = \frac{0.222(s - 0.00124)(s + 0.2695 \pm j1.675)}{(s - 2.017)(s + 0.0562)(s + 2.492 \pm j1.834)}$$

$$p24 = \frac{0.201(s - 0.00124)(s + 0.2686 \pm j1.645)}{(s + 2.017)(s + 0.0562)(s + 2.492 \pm j1.834)}$$

$$p25 = \frac{-0.222(s - 0.00124)(s + 0.2695 \pm j1.675)}{(s + 2.017)(s + 0.0562)(s + 2.492 \pm j1.834)}$$

$$p26 = \frac{-0.201(s - 0.00124)(s + 0.2686 \pm j1.645)}{(s + 2.017)(s + 0.0562)(s + 2.492 \pm j1.834)}$$

$$p27 = \frac{0.111(s - 0.00124)(s + 0.2706 \pm j1.712)}{(s + 2.017)(s + 0.0562)(s + 2.492 \pm j1.834)}$$

$$p28 = \frac{-0.111(s - 0.00124)(s + 0.2706 \pm j1.712)}{(s + 2.017)(s + 0.0562)(s + 2.492 \pm j1.834)}$$

$$p29 = \frac{0.115(s + 3.298)(s - 3.239)(s - 0.00125)}{(s + 2.017)(s + 0.0562)(s + 2.492 \pm j1.834)}$$

Yaw Rate Transfer Functions

$$p31 = \frac{0.049(s + 1.729)(s + 0.1838 \pm j0.7910)}{(s + 2.017)(s + 0.0562)(s + 2.492 \pm j1.834)}$$

$$p32 = \frac{-0.049(s + 1.729)(s + 0.1838 \pm j0.7910)}{(s + 2.017)(s + 0.0562)(s + 2.492 \pm j1.834)}$$

$$p33 = \frac{0.003(s + 0.9521)(s - 2.971 \pm j2.802)}{(s + 2.017)(s + 0.0562)(s + 2.492 \pm j1.834)}$$

$$p34 = \frac{0.002(s + 0.9250)(s - 0.6015 \pm j3.217)}{(s + 2.017)(s + 0.0562)(s + 2.492 \pm j1.834)}$$

$$p35 = \frac{-0.003(s + 0.9521)(s - 2.971 \pm j2.802)}{(s + 2.017)(s + 0.0562)(s + 2.492 \pm j1.834)}$$

$$p36 = \frac{-0.002(s + 0.9250)(s - 0.6015 \pm j3.217)}{(s + 2.017)(s + 0.0562)(s + 2.492 \pm j1.834)}$$

$$p37 = \frac{0.002(s + 0.9862)(s - 0.0921 \pm j2.449)}{(s + 2.017)(s + 0.0562)(s + 2.492 \pm j1.834)}$$

$$p38 = \frac{-0.002(s + 0.9862)(s - 0.0921 \pm j2.449)}{(s + 2.017)(s + 0.0562)(s + 2.492 \pm j1.834)}$$

$$p39 = \frac{-0.054(s + 1.902)(s + 0.1190 \pm j0.6434)}{(s + 2.017)(s + 0.0562)(s + 2.492 \pm j1.834)}$$

Appendix D. *Effective $p_{ii}(w\prime)$ Open Loop Transfer Functions for Nominal ACM Entry Case*

Continuous actuator dynamics of $(57.3)\left(\frac{20}{s+20}\right)$ are cascaded with each plant transfer functions after incorporation of the weighting matrix. The resulting effective plant transfer functions are transformed to the $w\prime$ plane. The sample rate is 80 Hz.

$$p_{11}(w\prime) = \frac{1.4916 \cdot 10^{-3} w\prime (w\prime + 3723)(w\prime + 0.00969)(w\prime + 1.07)(w\prime - 160)}{(w\prime - 19.9)(w\prime - 3.37)(w\prime - 1.6494)(w\prime + 0.00402 \pm j0.0356)}$$

$$p_{12}(w\prime) = 0$$

$$p_{13}(w\prime) = 0$$

$$p_{21}(w\prime) = 0$$

$$p_{22}(w\prime) = \frac{-1.1595 \cdot 10^{-3}(w\prime + 3491)(w\prime - 0.00125)(w\prime - 160)(w\prime + 0.2763 \pm j1.890)}{(w\prime + 19.9)(w + 2.017)(w\prime + 0.0562)(w\prime + 0.2492 \pm j1.834)}$$

$$p_{23}(w\prime) = \frac{-2.1832 \cdot 10^{-3}(w\prime + 3539)(w\prime - 0.00125)(w\prime - 160)(w\prime + 0.4266 \pm 3.989)}{(w\prime + 19.9)(w\prime + 2.017)(w\prime + 0.0562)(w\prime + 0.2492 \pm j1.834)}$$

$$p_{31}(w\prime) = 0$$

$$p_{32}(w\prime) = \frac{-4.5543 \cdot 10^{-5}(w\prime + 3657)(w\prime 1.150)(w\prime - 160)(w\prime + 0.2002 \pm j1.645)}{(w\prime + 19.9)(w\prime + 2.017)(w\prime + 0.0562)(w\prime + 0.2492 \pm j1.834)}$$

$$p_{33}(w\prime) = \frac{-1.0022 \cdot 10^{-3}(w\prime + 3750)(w\prime + 1.710)(w\prime - 160)(w\prime + 0.1785 \pm j0.8124)}{(w\prime + 19.9)(w\prime + 2.017)(w\prime + 0.0562)(w\prime + 0.2492 \pm j1.834)}$$

Appendix E. *Effective $q_{ii}(w\prime)$ Open Loop Transfer Functions for Nominal ACM Entry Case*

Continuous actuator dynamics of $(57.3)(\frac{20}{s+20})$ are cascaded with the plant transfer functions in the s plane before transformation to the $w\prime$ plane.

$$q_{11}(w\prime) = \frac{1.4916 \cdot 10^{-3} w\prime(w\prime - 3723)(w\prime + 0.00969)(w\prime + 1.070)(w\prime - 160)}{(w\prime - 19.9)(w\prime + 3.369)(w\prime - 1.6494)(w\prime - 0.004018 \pm j0.03561)}$$

$$q_{12}(w\prime) = \infty$$

$$q_{13}(w\prime) = \infty$$

$$q_{21}(w\prime) = \infty$$

$$q_{22}(w\prime) = \frac{1.0603 \cdot 10^{-3} w\prime(w\prime + 3489)(w\prime + 0.0628 \pm j0.0007)(w\prime - 160)}{(w\prime + 19.9)(w\prime - 0.0562)(w + 1.713)(w\prime + 0.1785 \pm j0.8124)}$$

$$q_{23}(w\prime) = \frac{-4.867 \cdot 10^{-4} w\prime(w\prime + 3757)(w\prime + 0.0628 \pm j0.0007)(w\prime - 160)}{(w\prime + 19.9)(w\prime - 0.001255)(w\prime - 0.0562)(w\prime + 0.4266 \pm j3.989)}$$

$$q_{31}(w\prime) = \infty$$

$$q_{32}(w\prime) = \frac{-2.3332 \cdot 10^{-2} w\prime(w\prime + 3489)(w\prime + 0.0628 \pm j0.0007)(w\prime - 160)}{(w\prime + 19.9)(w\prime - 1.15)(w\prime - 0.0562)(w\prime + 0.2002 \pm j1.645)}$$

$$q_{33}(w\prime) = \frac{9.1645 \cdot 10^{-4} w\prime(w\prime + 3757)(w\prime + 0.0628 \pm j0.0007)(w\prime - 160)}{(w\prime + 19.9)(w\prime - 0.001245)(w\prime - 0.0562)(w\prime + 0.2763 \pm j1.89)}$$

Appendix F. *Loop Transmission Characteristics*

Pitch Rate Loop

The following table displays the magnitude and phase angle obtained for the pitch rate loop transmission function.

Frequency	Magnitude (dB)	Phase Angle (degrees)
0.001	12.226	-163.108
0.002	12.895	-147.158
0.004	14.981	-120.166
0.008	20.247	-85.087
0.016	30.127	-54.898
0.032	49.934	-68.793
0.064	43.764	-179.592
0.128	41.241	-176.455
0.256	40.716	-168.212
0.512	40.626	-157.601
1.024	40.403	-141.469
2.048	38.64	-126.717
4.096	34.03	-117.909
8.192	27.613	-113.135
16.384	20.314	-111.092
32.768	12.252	-104.788
65.536	4.798	-87.154
131.07	-0.559	-62.128
262.14	-3.423	-37.879
524.29	-4.486	-21.294
1048.6	-4.797	-12.999
2097.2	-4.939	-11.110
4194.3	-5.426	-14.599
8388.6	-6.900	-18.423
16777	-8.601	-15.386
33554	-9.475	-9.3000
67109	-9.757	-4.911
134218	-9.859	0

Roll Rate Loop

The following table displays the magnitude and phase angle obtained for the roll rate loop transmission function.

Frequency	Magnitude (dB)	Phase Angle (degrees)
0.001	42.805	-177.314
0.002	42.807	-174.629
0.004	42.817	-169.270
0.008	42.855	-158.640
0.016	43.005	-138.040
0.032	43.561	-101.371
0.064	45.265	-50.153
0.128	48.715	-5.006
0.256	53.202	16.854
0.512	59.405	17.995
1.024	62.992	-118.365
2.048	46.577	-138.503
4.096	35.387	-138.976
8.192	25.529	-131.623
16.384	16.724	-122.700
32.768	8.127	-110.832
65.536	0.471	-89.186
131.07	-4.911	-60.435
262.14	-7.559	-31.793
524.29	-7.875	-10.360
1048.6	-6.784	-1.227
2097.2	-5.996	-5.565
4194.3	-6.654	-13.744
8388.6	-8.251	-18.089
16777	-9.985	-15.929
33554	-10.983	-10.062
67109	-11.328	-5.402
134218	-11.456	0

Yaw Rate Loop

The following table displays the magnitude and phase angle obtained for the yaw rate loop transmission function.

Frequency	Magnitude (dB)	Phase Angle (degrees)
0.001	96.816	-319.097
0.002	93.446	-297.519
0.004	88.437	-278.382
0.008	82.657	-260.936
0.016	76.490	-238.552
0.032	69.867	-199.679
0.064	66.205	-124.409
0.128	67.379	-135.704
0.256	57.324	-116.87
0.512	50.963	-91.508
1.024	47.708	-67.671
2.048	54.564	-160.542
4.096	29.870	-162.274
8.192	19.325	-134.623
16.384	11.397	-117.759
32.768	4.002	-104.754
65.536	-2.550	-90.188
131.07	-7.770	-76.043
262.14	-11.801	-67.715
524.29	-15.929	-67.046
1048.6	-20.859	-65.497
2097.2	-25.763	-56.156
4194.3	-29.378	-39.487
8388.6	-31.125	-22.939
16777	-31.702	-12.028
33554	-31.859	-6.092
67109	-31.899	-3.056
134218	-31.913	0

Appendix G. *Simulation Results*

ACM Entry Condition

Small Magnitude Pitch Rate Command Response The commanded pitch rate has a magnitude of 2 degrees/second and a duration of three seconds.
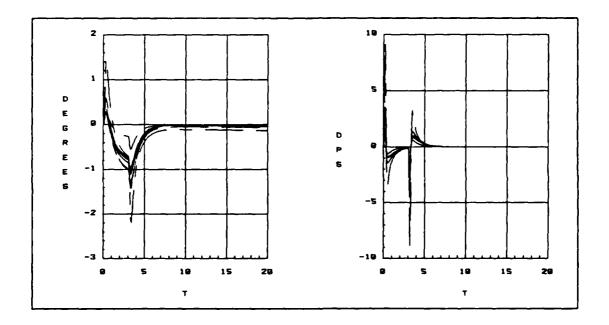
Figure G.1. Left Canard Position and Rate Deflection of 25 Cases for ACM Entry
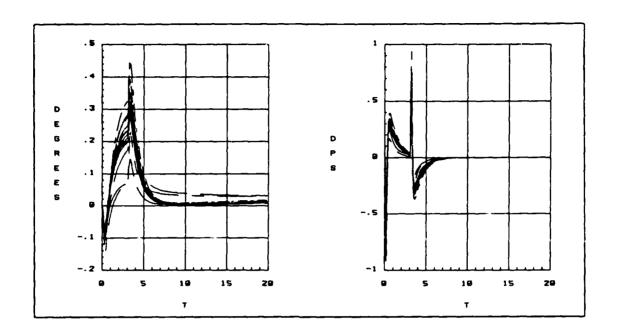
Figure G.2.   Left Outer Flap Position and Rate Deflection of 25 Cases for ACM
Entry
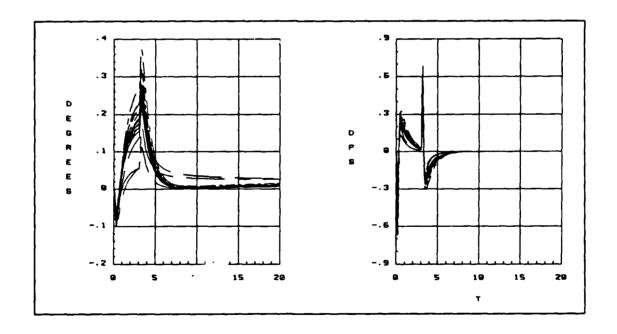
Figure G.3.   Left Inner Flap Position and Rate Deflection of 25 Cases for ACM
Entry
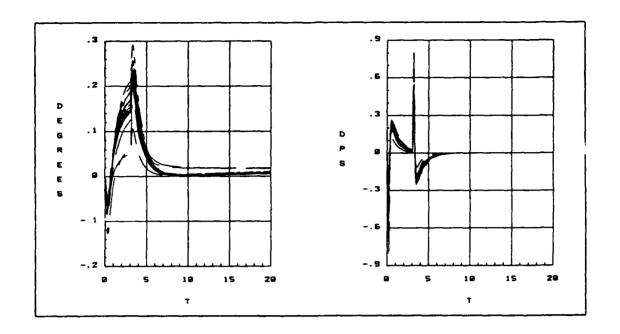
Figure G.4. Left Elevator Position and Rate Deflection of 25 Cases for ACM Entry
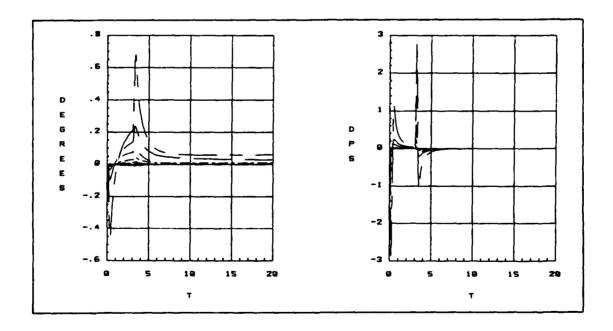
Figure G.5. Rudder Position and Rate Deflection of 25 Cases for ACM Entry
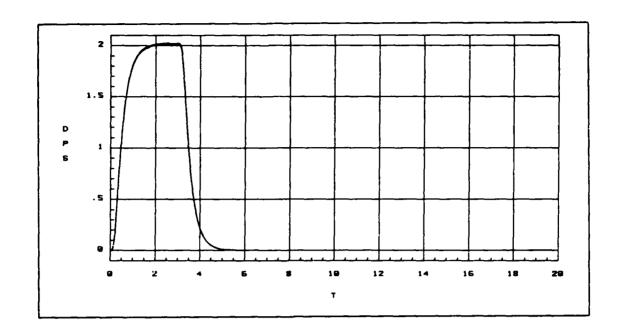
Figure G.6. Pitch Rate Response for 25 Cases for ACM Entry
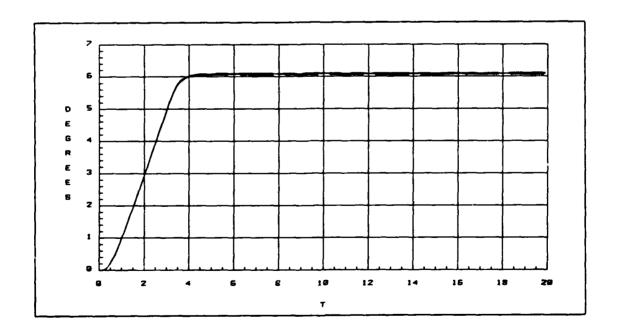
Figure G.7. Pitch Angle (θ) for 25 Cases for ACM Entry
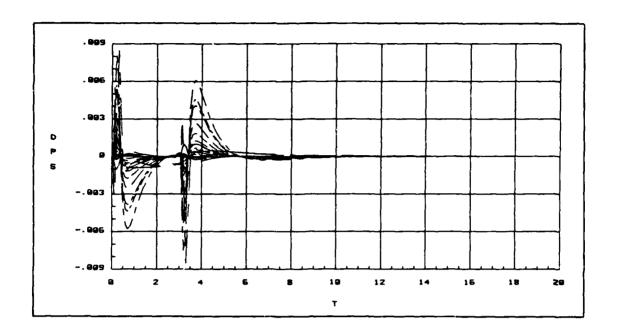
Figure G.8. Roll Rate Response for 25 Cases for ACM Entry
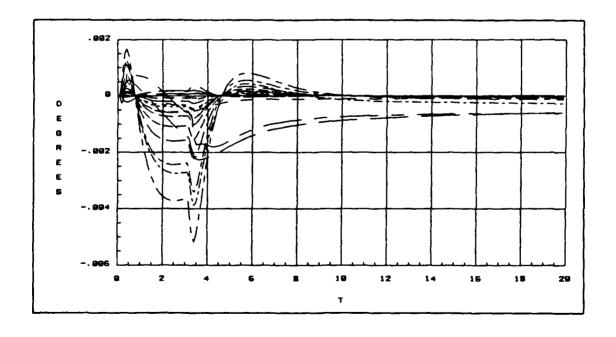
Figure G.9. Bank Angle (ϕ) for 25 Cases for ACM Entry

G-5
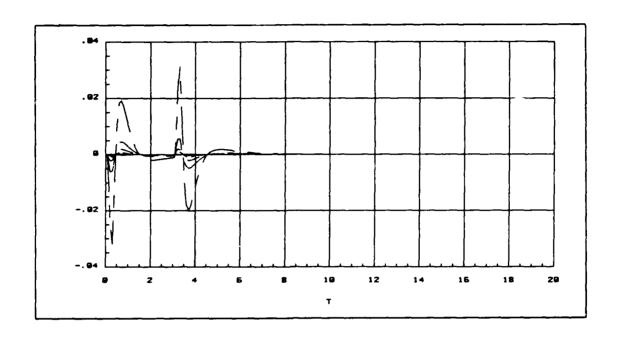
Figure G.10. Yaw Rate Response for 25 Cases for ACM Entry
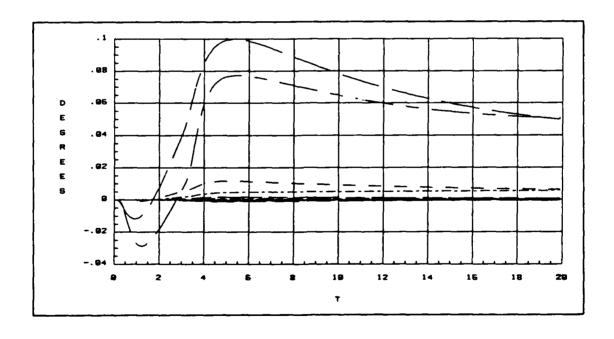
Figure G.11. Sideslip (β) for 25 Cases for ACM Entry

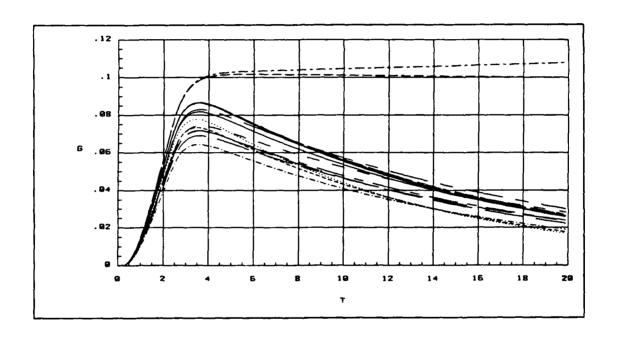G-6
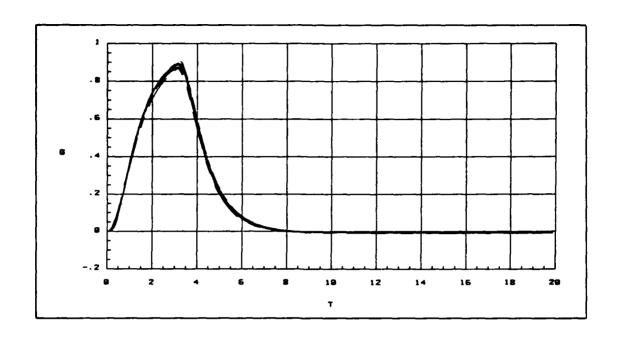
Figure G.12. Normal Acceleration for 25 Cases for ACM Entry
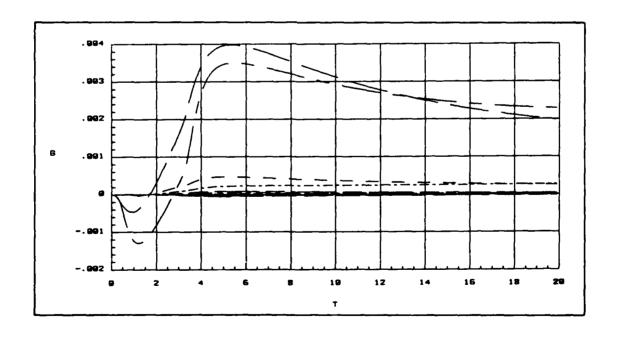
Figure G.13. Lateral Acceleration for 25 Cases for ACM Entry

Large Magnitude Pitch Rate Command Response The commanded pitch rate has a magnitude of 12 degrees/second and a duration of three seconds.
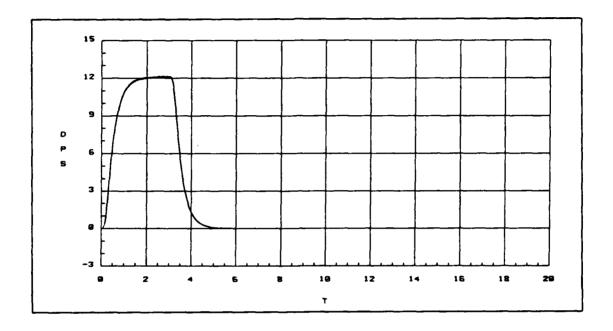
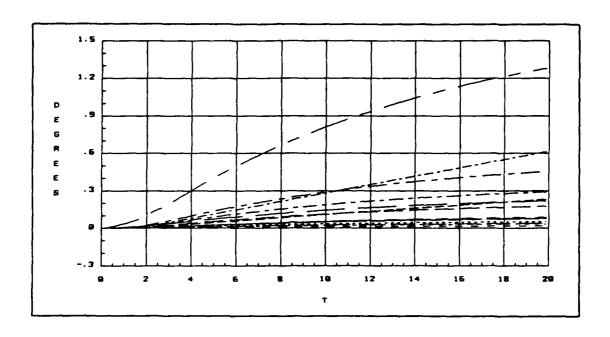Figure G.14. Pitch Rate Response for 25 Cases for ACM Entry
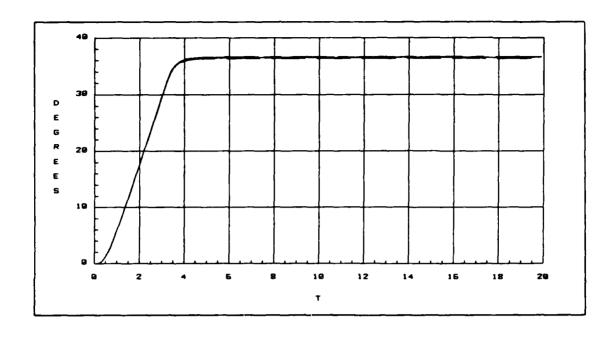
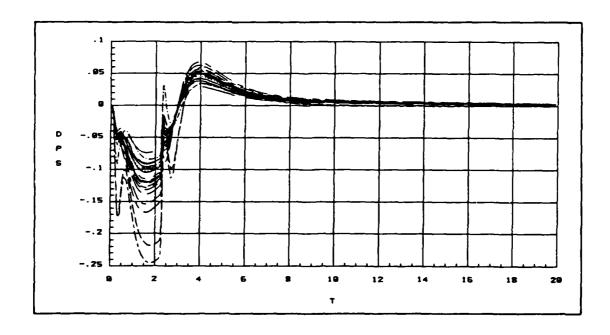Figure G.15. Pitch Angle (θ) for 25 Cases for ACM Entry
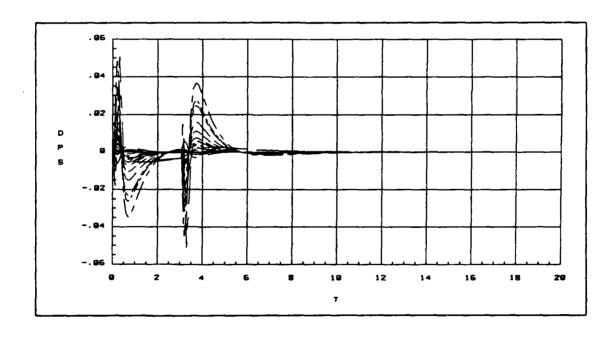
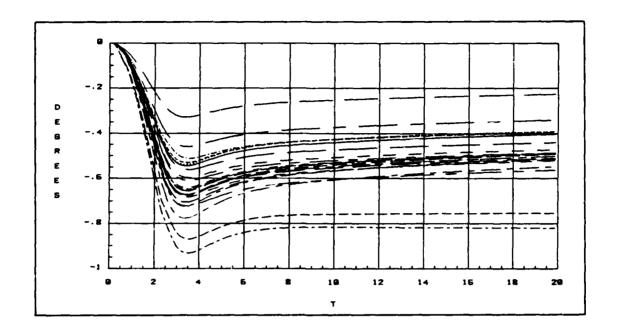Figure G.16. Roll Rate Response for 25 Cases for ACM Entry
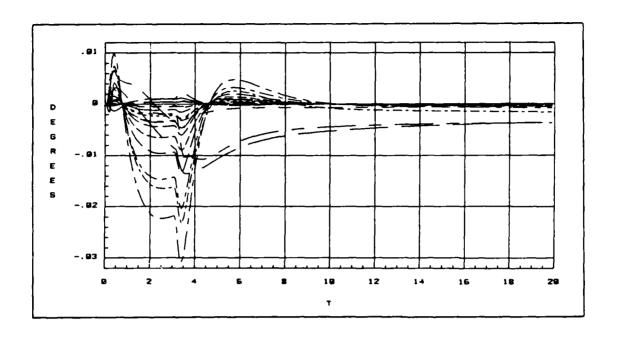
Figure G.17. Bank Angle (ϕ) for 25 Cases for ACM Entry
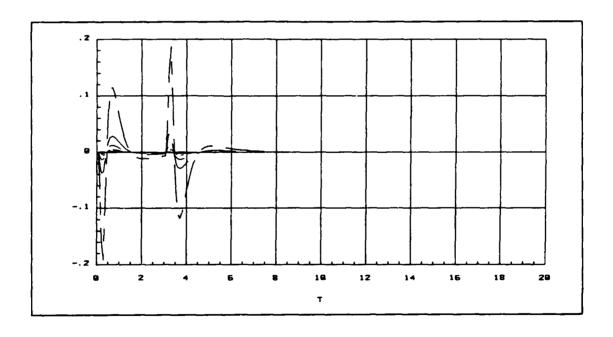
Figure G.18. Yaw Rate Response for 25 Cases for ACM Entry
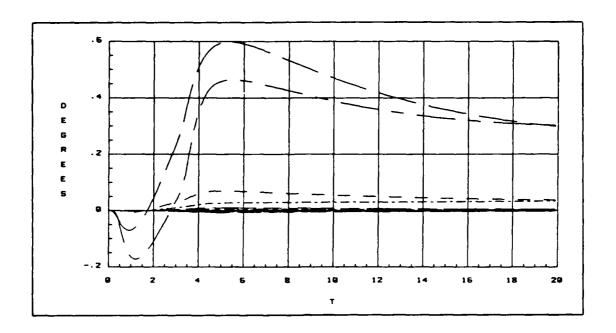
Figure G.19. Sideslip (β) for 25 Cases for ACM Entry
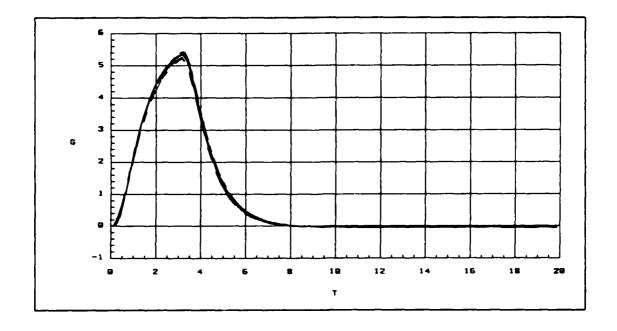
Figure G.20. Normal Acceleration for 25 Cases for ACM Entry
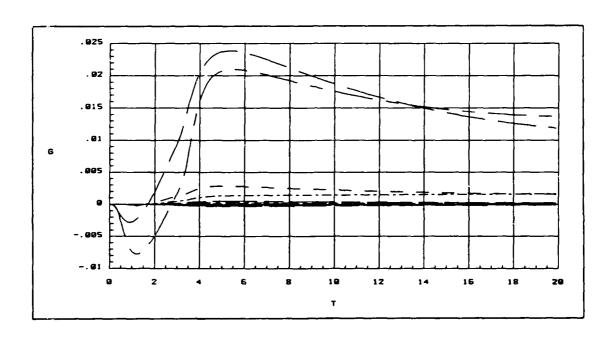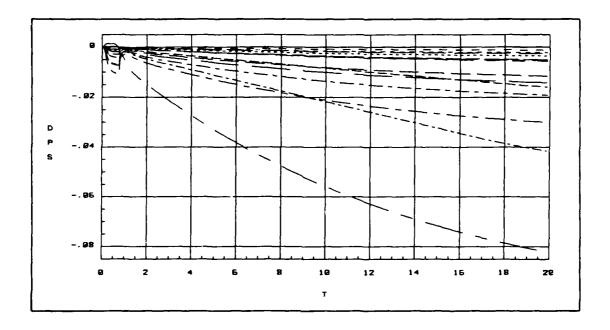
Figure G.21. Lateral Acceleration for 25 Cases for ACM Entry

Small Magnitude Roll Rate Command Response The commanded roll rate has a magnitude of 30 degrees/second and a duration of 0.5 seconds.

Figure G.22. Pitch Rate Response for 25 Cases for ACM Entry
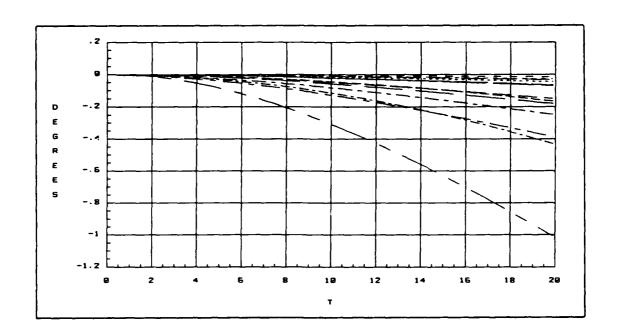
Figure G.23. Pitch Angle (θ) for 25 Cases for ACM Entry
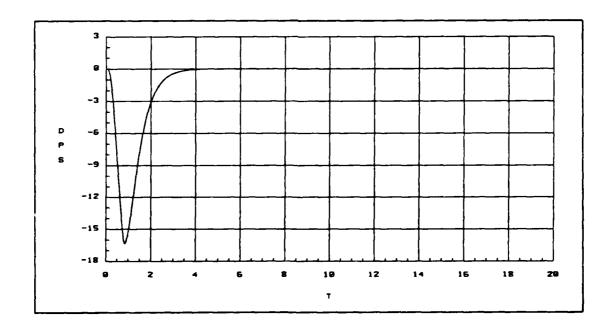
Figure G.24. Roll Rate Response for 25 Cases for ACM Entry
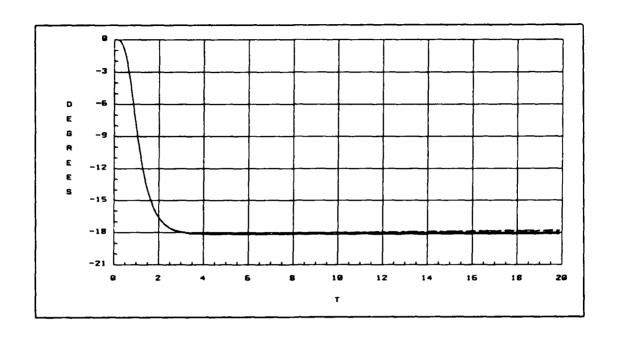
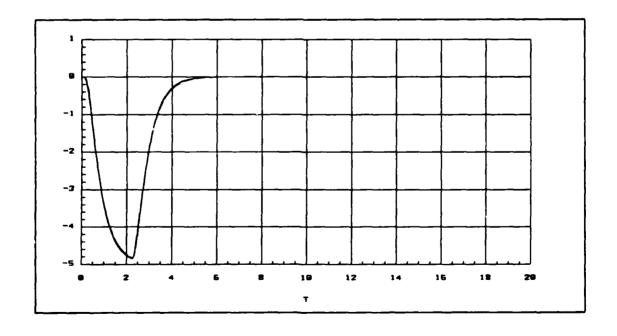Figure G.25. Bank Angle (ϕ) for 25 Cases for ACM Entry
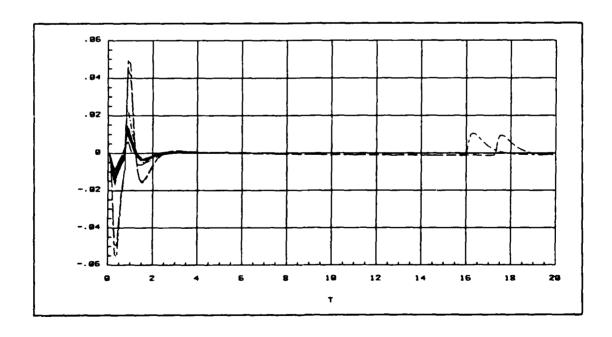
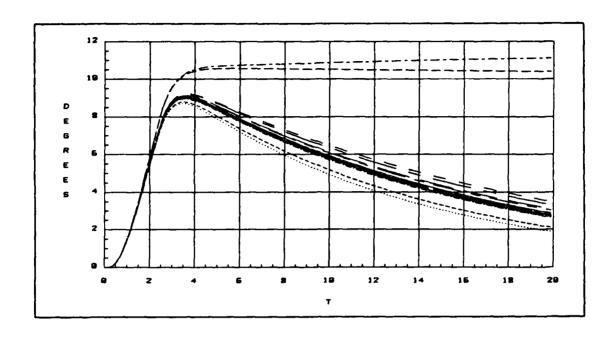Figure G.26. Yaw Rate Response for 25 Cases for ACM Entry
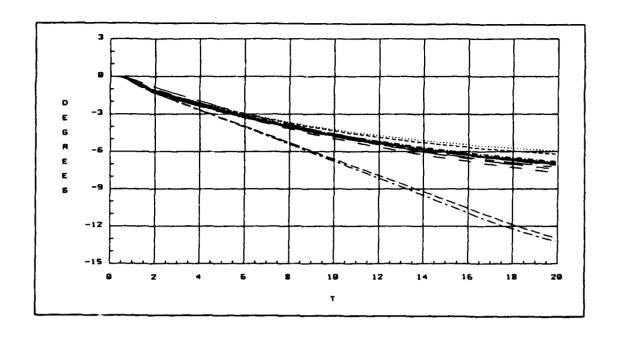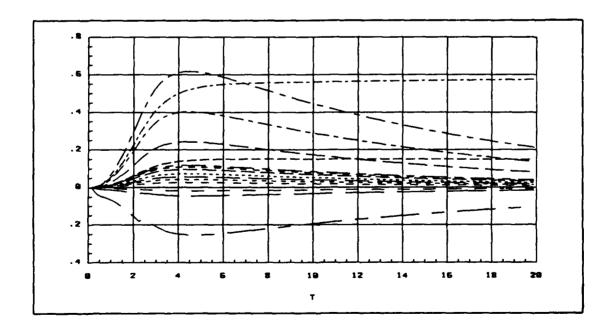
Figure G.27. Sideslip (β) for 25 Cases for ACM Entry
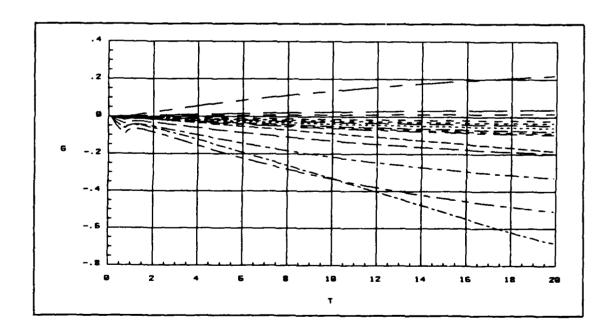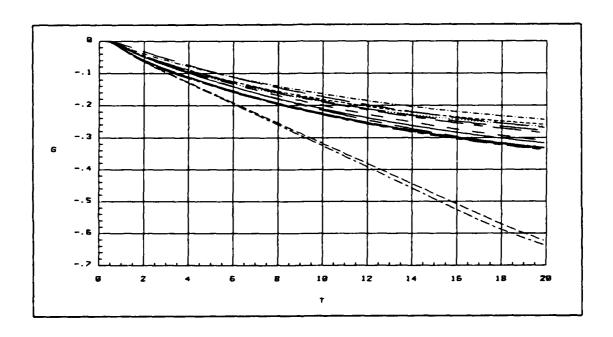
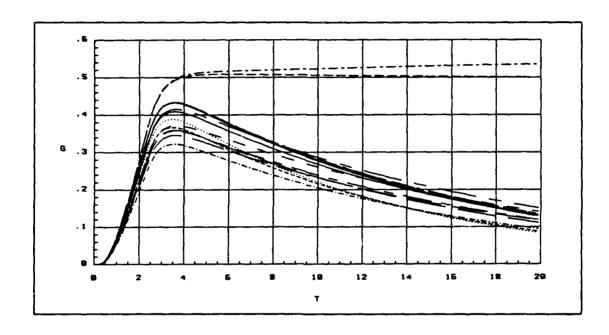Figure G.28. Normal Acceleration for 25 Cases for ACM Entry

G-16
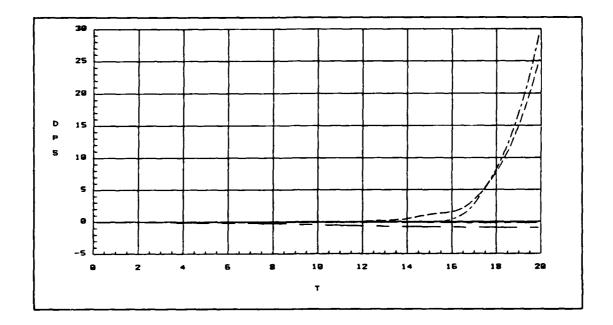
Figure G.29. Lateral Acceleration for 25 Cases for ACM Entry

Large Magnitude Roll Rate Command Response The commanded roll rate has a magnitude of 135 degrees second and a duration of 0.5 seconds.

Figure G.30. Pitch Rate Response for 25 Cases for ACM Entry
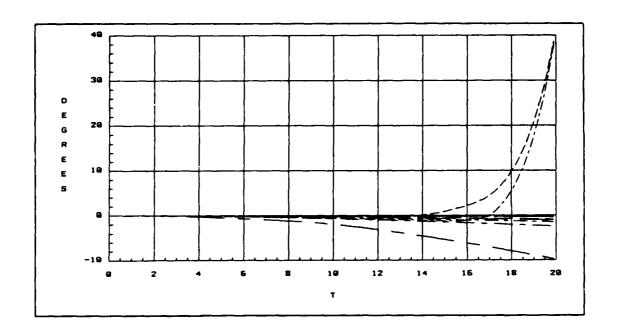
Figure G.31. Pitch Angle (θ) for 25 Cases for ACM Entry
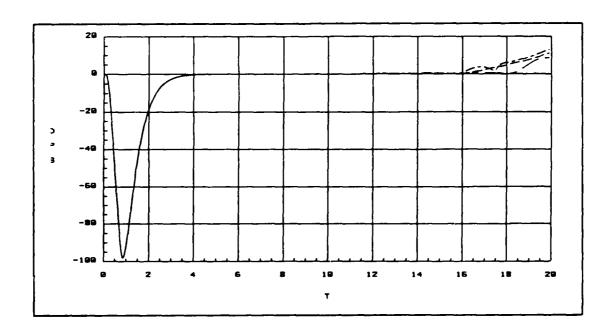
Figure G.32. Roll Rate Response for 25 Cases for ACM Entry
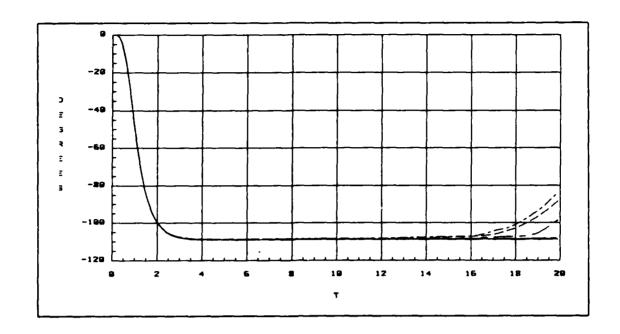
Figure G.33. Bank Angle (ϕ) for 25 Cases for ACM Entry
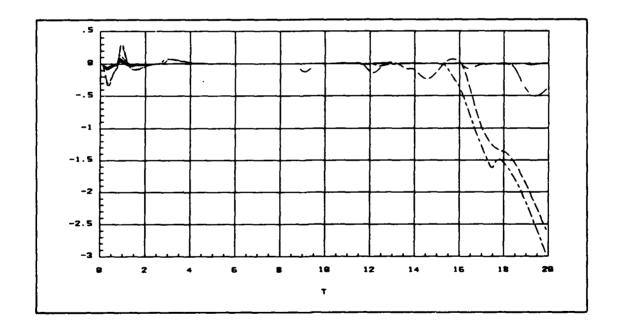
Figure G.34. Yaw Rate Response for 25 Cases for ACM Entry
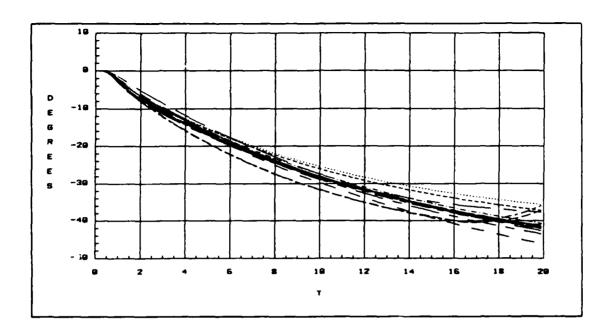
Figure G.35. Sideslip (β) for 25 Cases for ACM Entry
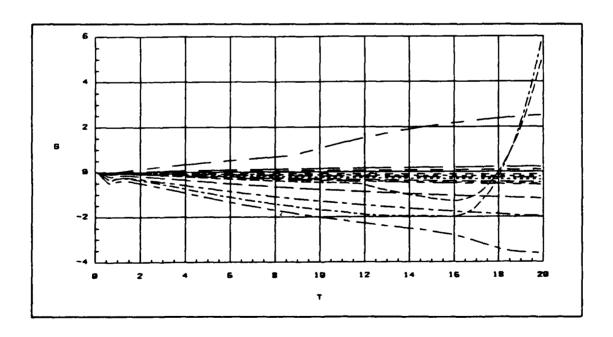
Figure G.36. Normal Acceleration for 25 Cases for ACM Entry

G-21
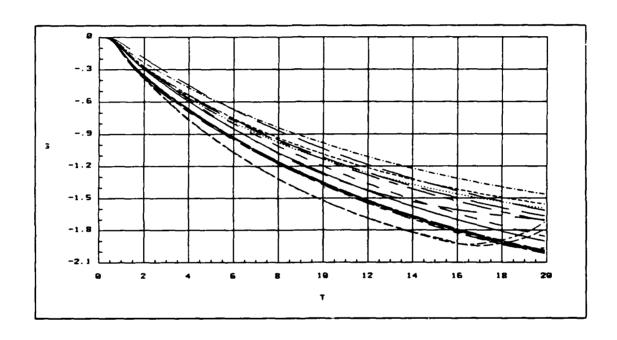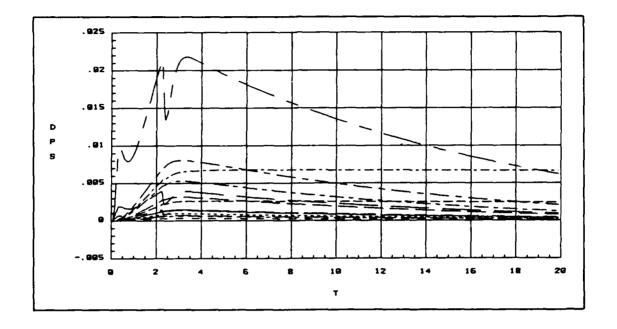
Figure G.37. Lateral Acceleration for 25 Cases for ACM Entry

Small Magnitude Yaw Rate Command Response The commanded yaw rate has a magnitude of 1 degree/second and a duration of two seconds.

Figure G.38. Pitch Rate Response for 25 Cases for ACM Entry
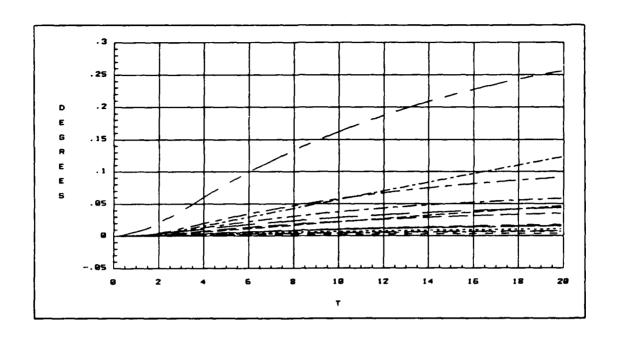
Figure G.39. Pitch Angle (θ) for 25 Cases for ACM Entry
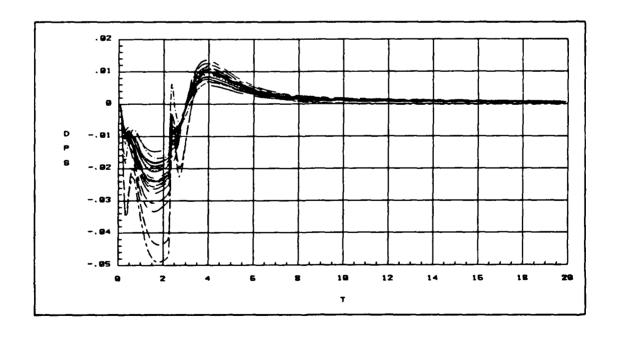
Figure G.40. Roll Rate Response for 25 Cases for ACM Entry
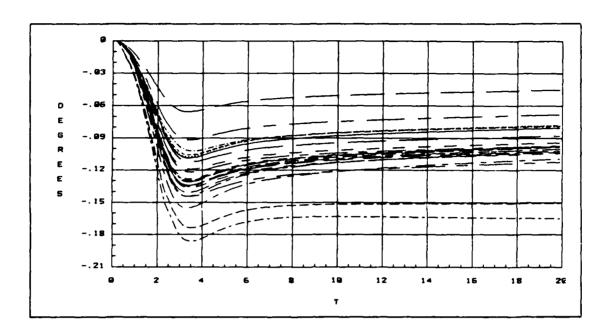
Figure G.41. Bank Angle (ϕ) for 25 Cases for ACM Entry
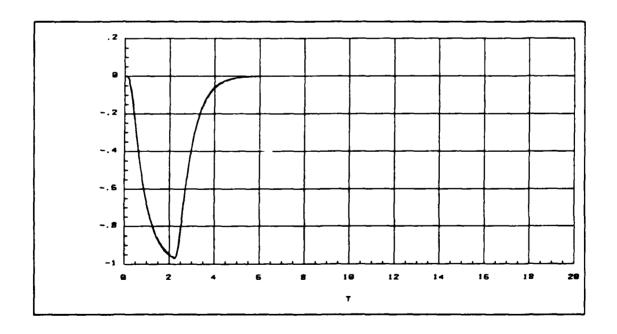
Figure G.42. Yaw Rate Response for 25 Cases for ACM Entry
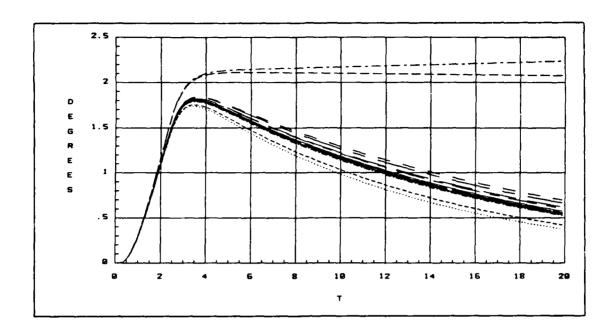
Figure G.43. Sideslip (β) for 25 Cases for ACM Entry
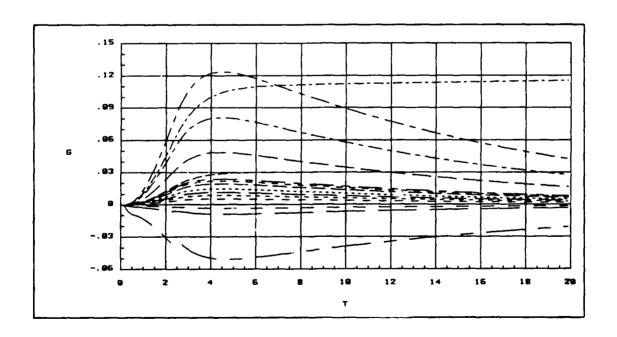
Figure G.44. Normal Acceleration for 25 Cases for ACM Entry

G-26
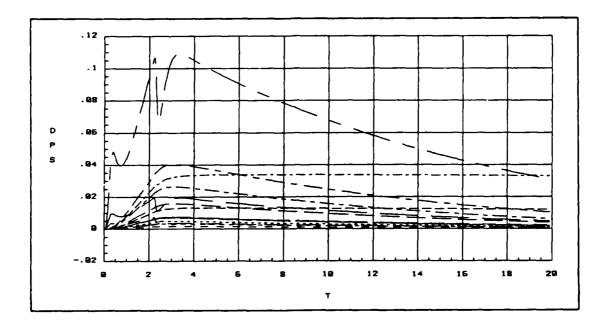
Figure G.45. Lateral Acceleration for 25 Cases for ACM Entry

Large Magnitude Yaw Rate Command Response The commanded yaw rate has a magnitude of 5 degrees /second and a duration of two seconds.

Figure G.46. Pitch Rate Response for 25 Cases for ACM Entry

Figure G.47. Pitch Angle (θ) for 25 Cases for ACM Entry

Figure G.48. Roll Rate Response for 25 Cases for ACM Entry

G-29

Figure G.49. Bank Angle (ϕ) for 25 Cases for ACM Entry

Figure G.50. Yaw Rate Response for 25 Cases for ACM Entry

G-30

Figure G.51. Sideslip (β) for 25 Cases for ACM Entry

Figure G.52. Normal Acceleration for 25 Cases for ACM Entry

G-31

Figure G.53. Lateral Acceleration for 25 Cases for ACM Entry

Coordinated Turn

The commanded pitch rate has a magnitude of 2 degrees/second, the commanded yaw rate has a magnitude of 2 degrees/second and the commanded roll rate has a magnitude of 2 degrees/second.
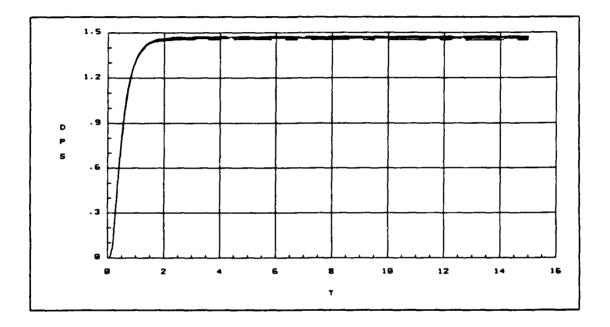
Figure G.54. Pitch Rate Response for 25 Cases for Coordinated Turn
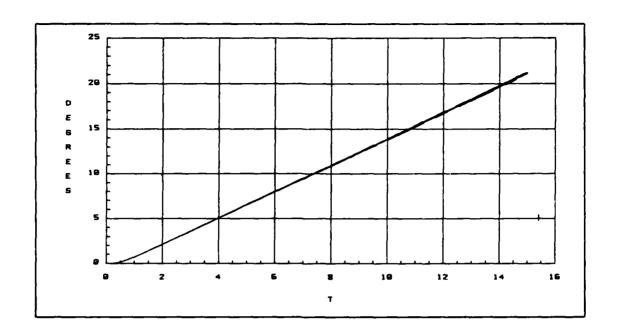
Figure G.55. Pitch Angle (θ) for 25 Cases for Coordinated Turn
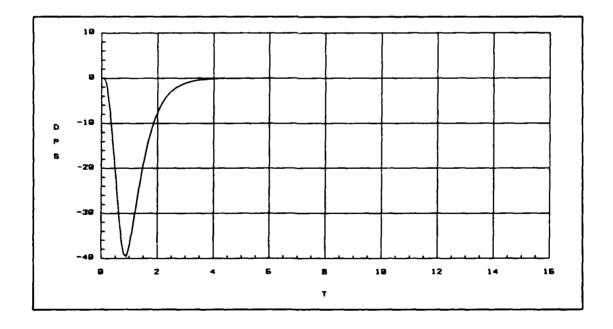
Figure G.56. Roll Rate Response for 25 Cases for Coordinated Turn
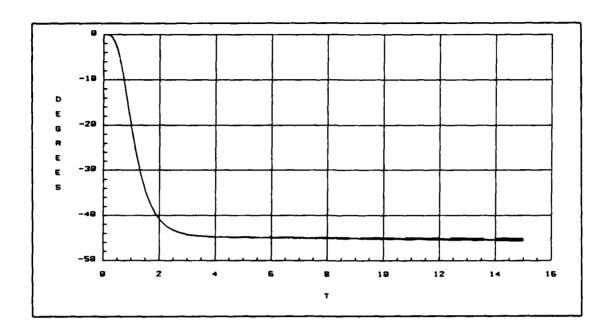
Figure G.57. Bank Angle (ϕ) for 25 Cases for Coordinated Turn
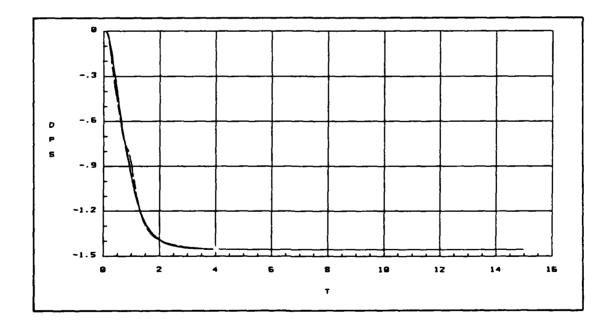
Figure G.58. Yaw Rate Response for 25 Cases for Coordinated Turn
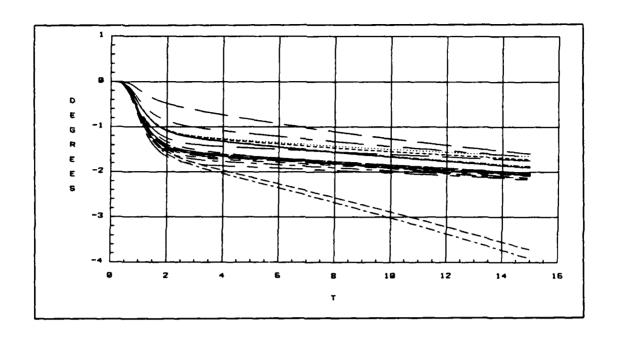
Figure G.59. Sideslip (β) for 25 Cases for Coordinated Turn
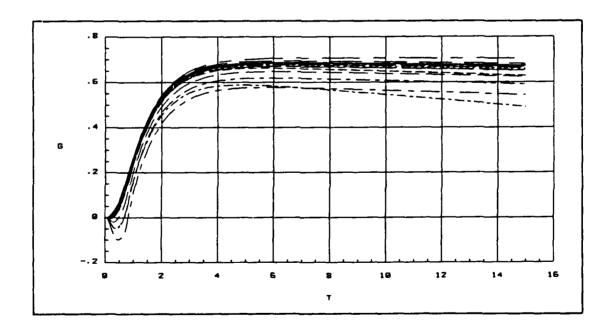
Figure G.60. Normal Acceleration for 25 Cases for Coordinated Turn

G-36
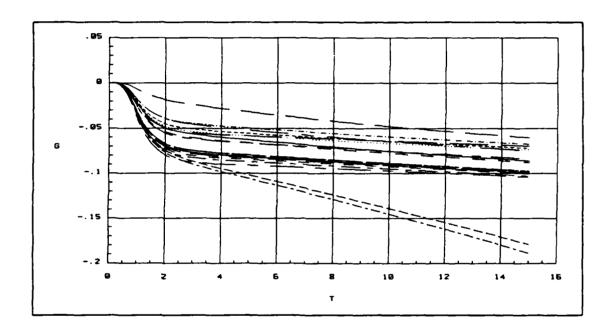
Figure G.61. Lateral Acceleration for 25 Cases for Coordinated Turn

Fourth Degree Actuators

   Pitch Rate Command The pitch rate command has a magnitude of 6 degrees/second and a duration of three seconds.
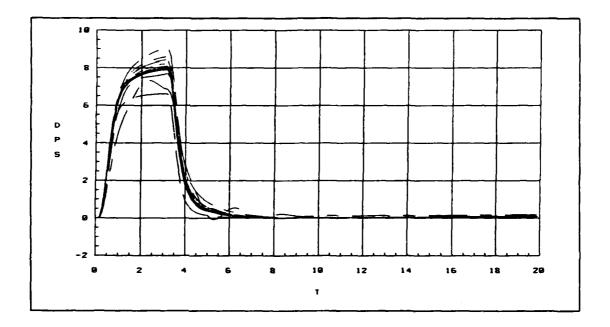
Figure G.62. Pitch Rate Response for 25 Cases with Fourth Degree Actuators
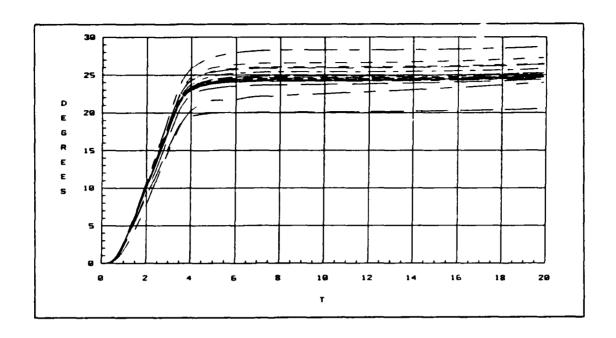
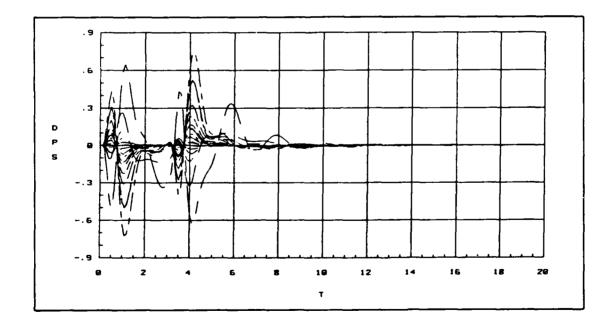Figure G.63. Pitch Angle (θ) for 25 Cases with Fourth Degree Actuators

Figure G.64. Roll Rate Response for 25 Cases with Fourth Degree Actuators
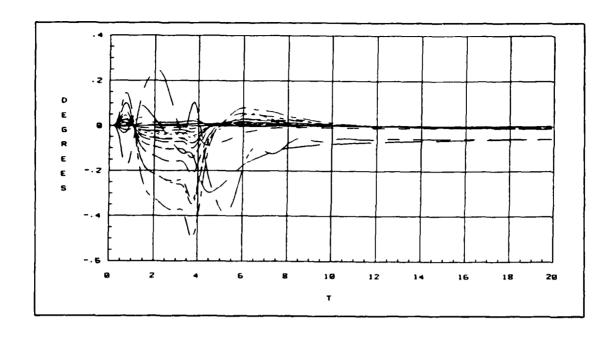
G-39

Figure G.65. Bank Angle (ϕ) for 25 Cases with Fourth Degree Actuators
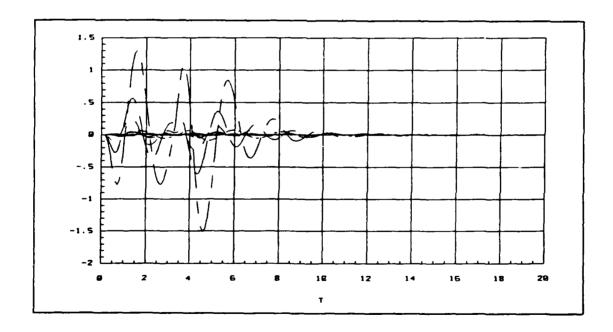

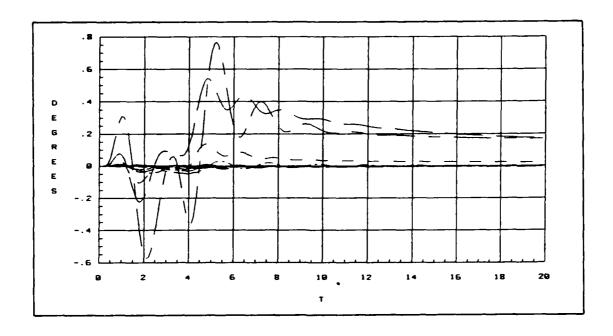Figure G.66. Yaw Rate Response for 25 Cases with Fourth Degree Actuators

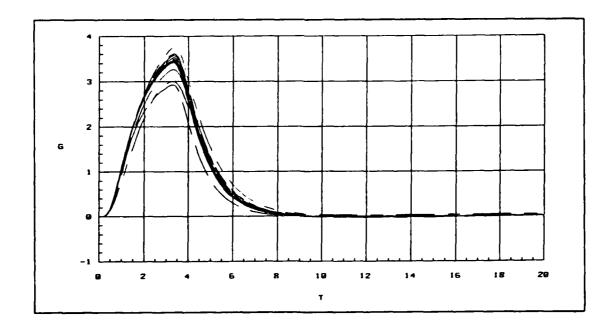Figure G.67. Sideslip (β) for 25 Cases with Fourth Degree Actuators
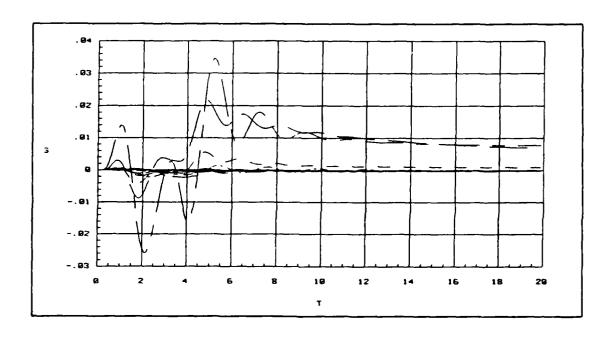

Figure G.68. Normal Acceleration for 25 Cases with Fourth Degree Actuators

G-41

Figure G.69. Lateral Acceleration for 25 Cases with Fourth Degree Actuators

Roll Rate Command The roll rate command has a magnitude of 90 degrees/second for 0.5 seconds.
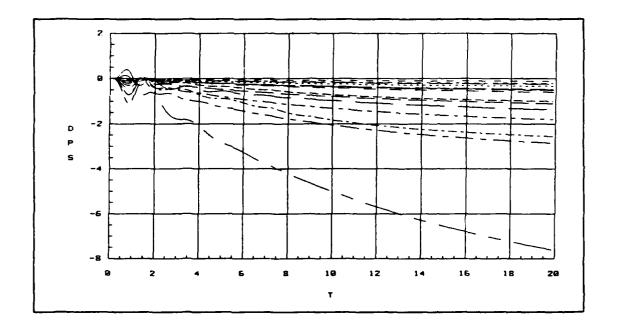

Figure G.70. Pitch Rate Response for 25 Cases with Fourth Degree Actuators

Figure G.71. Pitch Angle (θ) for 25 Cases with Fourth Degree Actuators
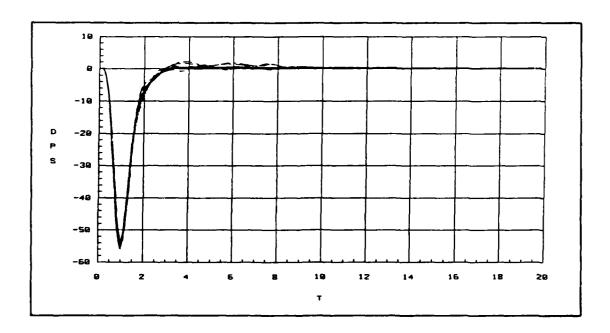
Figure G.72. Roll Rate Response for 25 Cases with Fourth Degree Actuators

G-44
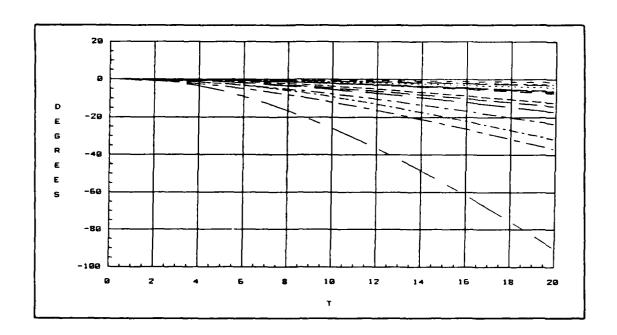
Figure G.73. Bank Angle (ϕ) for 25 Cases with Fourth Degree Actuators

Figure G.74. Yaw Rate Response for 25 Cases with Fourth Degree Actuators

G-45

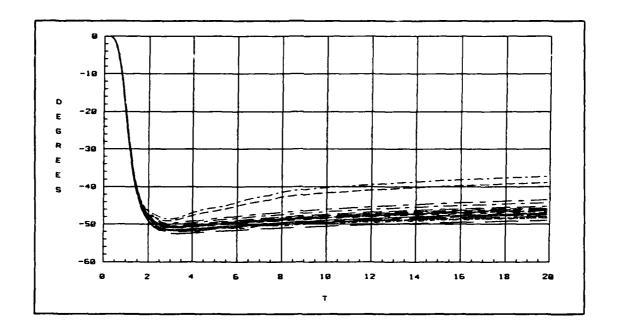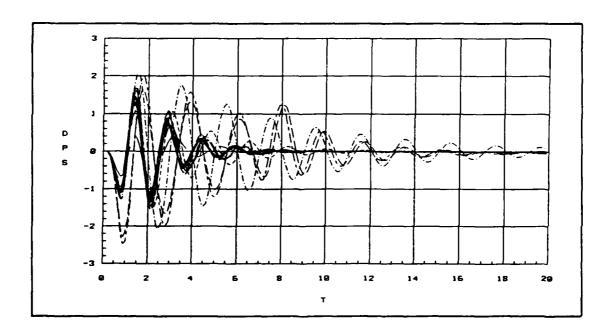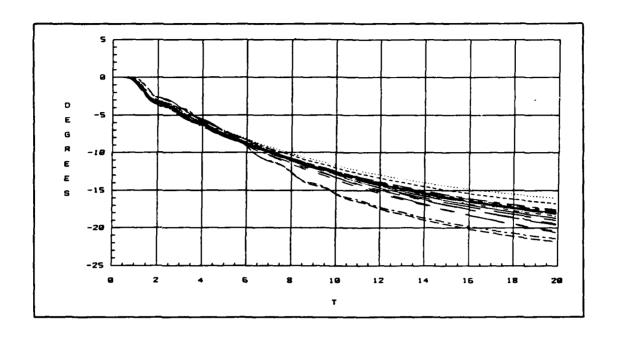Figure G.75. Sideslip (β) for 25 Cases with Fourth Degree Actuators
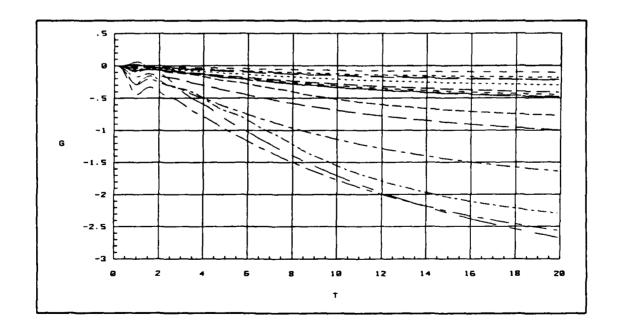

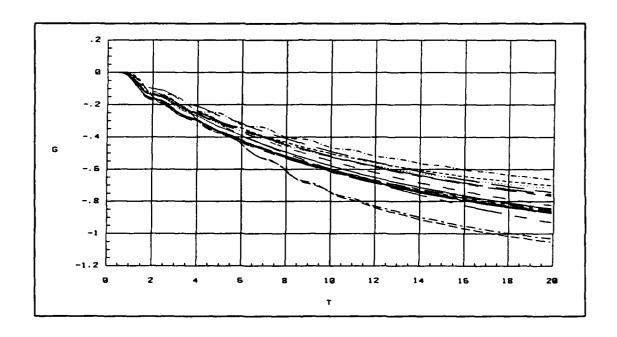Figure G.76. Normal Acceleration for 25 Cases with Fourth Degree Actuators

Figure G.77. Lateral Acceleration for 25 Cases with Fourth Degree Actuators

Bibliography

1. Adams, James M. *QFT Design of a Digital Controller for the AFTI/F-16 in the Longitudinal Mode.* MS Thesis, AFIT/GE/ENG/88M-4. School of Engineering, Air Force Institute of Technology (AU), Wright-Patterson AFB OH, March 1988.

2. Arnold, Phillip B. *Flight Control System Reconfiguration Using Quantitative Feedback Theory.* MS Thesis, AFIT/GE/ENG/84D-15. School of Engineering, Air Force Institute of Technology (AU), Wright-Patterson AFB OH, December 1984.

3. Barron, Roger L. *CRCA Linearized Equations of Motion and Closed Loop Simulations.* Interim Technical Report, Purchase Order 5035, F33615-84-C-3609. Barron Associates, Inc. September 1986.

4. Beaufree, Henry L., D. Alexander Stratton. and Shawn Soeder. *Control Power Requirements for Statically Unstable Aircraft.* AFWAL-TR-87-3018. Air Force Wright Aeronautical Laboratory, Wright-Patterson AFB OH, June,1987.

5. Chandler, Phillip R. and Duane P. Rubertus. *A System Approach to Flight Control Reliability and Maintainability.* AIAA-84-2463, Aircraft Design, Systems and Operations Meeting, San Diego, Oct-Nov.,1984.

6. D'azzo, John. J. and Constantine H. Houpis. *Linear Control System Analysis and Design, Third Edition.* New York: McGraw Hill, 1988.

7. Etkin, Benard. *Dynamics of Atmospheric Flight.* New York: John Wiley and Sons, Inc., 1972.

8. Hamilton, Steven W. *QFT Digital Controller for an Unmanned Research Vehicle with an Improved Method for Choosing the Control Weightings.* MS Thesis, AFIT/GE/ENG/87D-22. School of Engineering, Air Force Institute of Technology (AU), Wright-Patterson AFB OH, December 1987.

9. Hofmann, L.G. "Technique for Analysis of Digital Control Systems", General Electric Company, Avionic and Electronic Systems Division. Binghampton, New York.

10. Horowitz, Issac M. *Synthesis of Feedback Systems.* New York: Academic Press, 1963.

11. Horowitz, Isaac M. and Marcel Sidi. "Synthesis of Feedback Systems with Large Plant Ignorance for Prescribed Time-Domain Tolerances," *International Journal of Control*, 16 (20): 287-309 (1972).

12. Horowitz, Isaac M. and T. Kopelman. *Multivariable Flight Control Design with Uncertain Parameters.* Final Report. Department of Applied Mathematics, The Weizmann Institute of Science, Rehovt, Israel. September 1982.

13. Horowitz. Isaac M. "Improved Design Technique for Uncertain Multiple-Input. Multiple-Output Feedback Systems," *International Journal of Control.* 36 (6): 977-988 (1982).

14. Horowitz, Isaac M. and Oded Yaniv. "Quantitative Cascaded Multiple-Input, Multiple-Output Synthesis by an Improved Method," *International Journal of Control.* 42 (2): 305-311 (1985).

15. Horowitz. Isaac M., et al. *Research in Advanced Flight Control Designs.* AFFDL-TR-79-3120, Department of Applied Mathematics, the Weizmann Institute of Science, Renovot, Israel, January 1980.

16. Horowitz, Isaac M. and Claytin Loecher. "Design of a 3x3 Multivarible Feedback System with Large Plant Uncertainty", *International Journal of Control,* *30* (1): 677-699 (April 1981).

17. Horowitz. Isaac M. Conversation and Discussion. Department of Electrical Engineering, University of California, Davis. December 1986 to August 1987.

18. Horowitz, Isaac M. and Uri Shaked. "Superiority of Transfer Function Over State-Variable Methods in Linear Time-Invariant Feedback System Design", *IEEE Transactions, AC-20* (1): 84-97, (1975).

19. Houpis, Constantine H. Conversation and Discussion. Electrical and Computer Engineering Department, Air Force Institute of Technology, Wright-Patterson AFB OH, December 1986 to February 1988.

20. Houpis, Constantine H. and Gary B. Lamont. *Digital Control Systems: Theory, Hardware, Software.* New York: McGraw Hill, 1985.

21. Houpis, Constantine H. *Quantitative Feedback Theory Technique for Designing Multivariable Control Systems.* AFWAL-TR-86-3107. Air Force Wright Aeronautical Laboratory, Wright-Patterson AFB OH, January 1987.

22. Integrated Systems Inc. *MatrixX Users Guide, (Version 6.0).* Palo Alto, California, May 1986.

23. Kuo, Benjamin. *Digital Control Systems.* Champaign, Illinois: SRL Publishing Company, 1977.

24. McRuer, Duane, Richard Whitbeck, and Raymond Magdaleno. *Methodologies for the Direct Digital Control of Highly Flexible Structures.* AFWAL-TR-84-3104. Air Force Wright Aeronautical Laboratory, Wright-Patterson AFB OH, February 1985.

25. Schneider, Dean L. *QFT Digital Flight Control Design as Applied to the AFTI/F-16.* MS Thesis, AFIT/GE/ENG/86D-4. School of Engineering, Air Force Institute of Technology (AU), Wright-Patterson AFB OH, December 1986.

26. Weinstein. Warren. *Control Reconfigurable Combat Aircraft Development Phase I - R&D Design Evaluation*. AFWAL-TR-87-3011. Air Force Wright Aeronautical Laboratory, Wright-Patterson AFB OH, May 1987.

Vita

Captain Kurt N. Neumann attended the University of Colorado from September 1975 to May 1981. He received a Bachelor of Arts with a double major in Biochemistry and Cellular Biology. He entered USAF Officer Training School in May 1981. Captain Neumann's first assignment was at Auburn University where he received a Bachelor of Science in Electrical Engineering in August 1983. His second assignment was with the 6595 Shuttle Test Group at Vandenberg Air Force Base from September 1983 to May 1987. His present assignment is at the Air Force Institute of Technology in a master's program. Following graduation, Captain Neumann will be reassigned to the Flight Dyanimics Laboratory of the Wright Aeronautical Laboratories.

REPORT DOCUMENTATION PAGE

Form Approved
OMB No. 0704-0188

1a. REPORT SECURITY CLASSIFICATION UNCLASSIFIED	1b. RESTRICTIVE MARKINGS

2a. SECURITY CLASSIFICATION AUTHORITY	3. DISTRIBUTION / AVAILABILITY OF REPORT
2b. DECLASSIFICATION / DOWNGRADING SCHEDULE	Approved for public release; distribution unlimited.

4. PERFORMING ORGANIZATION REPORT NUMBER(S) AFIT/GE/ENG/88D-33	5. MONITORING ORGANIZATION REPORT NUMBER(S)

6a. NAME OF PERFORMING ORGANIZATION School of Engineering	6b. OFFICE SYMBOL (If applicable) AFIT/ENG	7a. NAME OF MONITORING ORGANIZATION

6c. ADDRESS (City, State, and ZIP Code) Air Force Institute of Technology Wright-Patterson AFB Ohio 45433	7b. ADDRESS (City, State, and ZIP Code)

8a. NAME OF FUNDING / SPONSORING ORGANIZATION AFWAL Flight Dynamics Lab	8b. OFFICE SYMBOL (If applicable) AFWAL/FDCLA	9. PROCUREMENT INSTRUMENT IDENTIFICATION NUMBER

8c. ADDRESS (City, State, and ZIP Code) Wright-Patterson AFB Ohio 45433	10. SOURCE OF FUNDING NUMBERS

PROGRAM ELEMENT NO.	PROJECT NO.	TASK NO.	WORK UNIT ACCESSION NO.

11. TITLE (Include Security Classification)
A Digital Rate Controller For the Control Reconfigurable Combat Aircraft Designed Using Quantitative Feedback Theory

12. PERSONAL AUTHOR(S)
Kurt Neumann, Captain, USAF

13a. TYPE OF REPORT Thesis	13b. TIME COVERED FROM _____ TO _____	14. DATE OF REPORT (Year, Month, Day) 1988 December	15. PAGE COUNT 143

16. SUPPLEMENTARY NOTATION

17. COSATI CODES			18. SUBJECT TERMS (Continue on reverse if necessary and identify by block number)
FIELD	GROUP	SUB-GROUP	Control Theory, Flight Control Systems, Multivariable Control, Quantitative Feedback Theory
01	04		

19. ABSTRACT (Continue on reverse if necessary and identify by block number)

Thesis Advisor: Dr C. H. Houpis

20. DISTRIBUTION / AVAILABILITY OF ABSTRACT ☒ UNCLASSIFIED/UNLIMITED ☐ SAME AS RPT. ☐ DTIC USERS	21. ABSTRACT SECURITY CLASSIFICATION UNCLASSIFIED
22a. NAME OF RESPONSIBLE INDIVIDUAL Constantine H. Houpis, Professor	22b. TELEPHONE (Include Area Code) (513) 255-3576	22c. OFFICE SYMBOL AFIT/ENG

DD Form 1473, JUN 86   Previous editions are obsolete.   SECURITY CLASSIFICATION OF THIS PAGE

UNCLASSIFIED

The objective of this thesis is to develop a digital controller
using Quantitative Feedback Theory (QFT) for a fighter aircraft with
unstable, nonminimum phase dynamics that meets performance
specifications despite surface failures. The three controlled states
are the pitch, roll, and yaw rates. A weighting matrix is derived
which linearly combines the nine control surfaces into three control
inputs. The plant is converted to the w' plane using the Hofmann
algorithm. Three constant gain controllers and three prefilters are
designed for a single flight condition of 0.9 Mach and 30000 ft
altitude. The controllers and prefilters are transformed to the z
plane for simulation purposes. The design is simulated with a healthy
plant and 24 combinations of surface failures. The failure cases
consisted of single and double surface impairments. The nonlinear
effects of rate and deflection limiters on the actuator models are
added to the simulations. The first set of simulations consist of
single channel inputs to determine the level of inertial decoupling. A
coordinated turn with 55 degrees of bank is simulated next. The first
order actuators are replaced with fourth order actuators and a digital
filter is cascaded with the digital controllers. The loop transmission
is nearly restored and a 2 degree/second pitch rate command and 90
degree/second roll command are simulated. An attempt to extend the
design to a second flight condition of 0.9 Mach and 200 ft is
unsuccessful.

The design is shown to meet design objectives in spite of surface
failures for all failure conditions in the longitudinal mode. Two
failure conditions are not satisfactorily controlled during the roll
rate commands. The replacement of the first order actuators with the
fourth order actuators is shown to be most successful in the
longitudinal mode. Excessive oscillatory behavior is found in the
lateral modes. Quantitative Feedback Theory is shown to be applicable
for sampled-data, multi-input, multi-output, unstable, and nonminimum
phase aircraft.